Mathematical Biosciences and Engineering

http://www.aimspress.com/journal/mbe

MBE, 23(8): 2323–2366.
DOI: 10.3934/mbe.2026085
Received: 05 March 2026
Revised: 04 May 2026
Accepted: 23 June 2026
Published: 24 July 2026

Research article

A virtual epidemics approach to HIV dynamics in the United States (1981–2030)

Necibe Tuncer[1,*], Yuganthi R. Liyanage[2], Vincent D. Holmlund[3] and Maia Martcheva[3]

[1] Department of Mathematics and Statistics, Florida Atlantic University, Boca Raton, FL 33431, USA
[2] School of Mathematical and Statistical Sciences, Arizona State University, Tempe, AZ 85287, USA
[3] Department of Mathematics, University of Florida, Gainesville, FL 32611, USA

* **Correspondence:** Email: ntuncer@fau.edu.

Abstract: The human immunodeficiency virus (HIV) epidemic in the United States has changed substantially since it was first identified in 1981; yet, progress toward ending the HIV epidemic targets remains uncertain. In this study, we examined the progress of the United States using HIV epidemic data from 1981 to 2025 and project trends through 2030 using mathematical transmission models. Two models were considered: A transmission model without pre-exposure prophylaxis (PrEP) and an extended model incorporating PrEP-related behavioral dynamics. Structural and practical identifiability analyses were used to assess whether model parameters could be reliably estimated from available surveillance data. Although both models were structurally identifiable under fixed assumptions, only the model without PrEP was practically identifiable with current surveillance data. We introduced the concept of virtual epidemics (VEs) and generated a collection of epidemic trajectories by repeatedly fitting the identifiable model to bootstrapped surveillance data. These VEs reproduced historical HIV incidence trends and yielded a range of plausible future outcomes. Our simulations suggested that, under current patterns of diagnosis, treatment, and prevention, the goal of reducing 90% of the HIV epidemic in new infections by 2030 was unlikely to be met without additional intervention efforts.

Keywords: virtual epidemics; evolutionary game theory; structural identifiability; practical identifiability; HIV

1. Introduction

Human immunodeficiency virus (HIV) continues to cause new infections in the United States and abroad, remaining a significant public health challenge. HIV originated in Africa in the early 1900s and was first discovered in the United States in 1981, and predominantly among men who have sex

with men (MSM) [1, 2]. Prior to the discovery of antiretroviral therapy (ART) drugs in the mid-1990s, HIV was a death sentence via its advanced form, acquired immunodeficiency syndrome (AIDS) [3, 4]. Fortunately, ART now enables many people with HIV to live long, normal lives [5]. Despite these advances, HIV still kills over 600,000 people worldwide each year, often because they are unaware of their infection or lack access to treatment [4].

Researchers started modeling HIV in the 1980s, shortly after the virus was identified [6]. Early models were inspired by the SIR models of Kermack and McKendrick, which have been around since the early 1900s [7]. Other so-called "Viral Dynamics" models track the spread of HIV within a patient [8]. Multiscale models combine viral dynamics with epidemiological models, and this approach determines how an individual's infection affects the wider disease course in the population [9].

Pre-exposure prophylaxis (PrEP) involves HIV-negative individuals taking prophylactic medications before potential exposure. This has been shown to reduce the risk of acquiring HIV [10]. For example, when taken as prescribed, oral PrEP lowers the risk of sexually transmitted HIV by 99% and injection-related HIV by 74% [10]. HIV incidence in the United States states depends highly on PrEP usage. For example, one study revealed a 38% decline in new HIV diagnoses over a decade (2012–2022) for states in the top quintile of PrEP usage. However, states with low PrEP coverage saw increases during the same period [11].

In 2019, the United States government launched the Ending HIV Epidemic 2030 initiative, which aims to reduce HIV incidence by 90% by 2030 [12]. CDC estimates show a 12% decline in incidence from 2018 to 2022, while states with the highest PrEP coverage observed a 38% decline [13, 14]. Despite these efforts, most estimates indicate that the United States will not achieve its goal of a 90% decline by 2030 [15].

Many researchers have used compartmental or ordinary differential equation models to track the spread of HIV with PrEP usage. In [16], the authors utilized a five-compartment model to simulate the spread of HIV among MSM in Cameroon. In another study [17], used a seven-compartment model to track the spread of HIV among MSM in South Korea. The authors determined that PrEP is the most effective prevention measure against HIV, surpassing early treatment and early diagnosis. The researchers in [18] found that while PrEP usage will be sufficient to eliminate HIV among populations of MSM with only long-term or casual partnerships, more interventions would be needed in populations with long- and short-term partnerships. Moreover, the researchers in [19] found that models with serosorting uncovered a greater PrEP impact than models without it.

Evolutionary game theory plays an important role in understanding the spread and control of infectious diseases by capturing the evolution of individual strategies and payoffs within a population [20]. In this context, human decisions are modeled by evaluating risks and benefits based on observed outcomes. We refer to this phenomenon as imitation dynamics. Imitation dynamics has been extensively studied in the context of vaccination [21]. However, few researchers have considered its influence on PrEP adoption in the context of HIV. In general, evolutionary game theory has been used to model biological phenomena, such as cancer growth and the effect of pharmaceuticals [20, 22, 23].

Virtual clinical trials have become a popular way to predict the performance of new cancer drugs in large populations [24, 25]. They enable simulations of drug testing in a large and diverse sample, beyond what conventional trials allow [25, 26]. Despite the advantages of this technique, studies have

revealed that virtual clinical trials may not be reliable if the model is not identifiable [27]. To our knowledge, this method has never been applied to simulate epidemics. Building on this gap, we aim to simulate a virtual HIV epidemic and determine whether the United States will meet its goal of EHE (Ending the HIV Epidemic) by 2030.

In this paper, we introduce a novel evolutionary game theoretic model of HIV and PrEP usage. In Section 2 we detail the behavior model and examine the existence and stability of its equilibria, with and without the behavioral component. In Section 3, we present structural identifiability results for the model and fit it to data. In Section 4, we use the model to generate virtual epidemics (VEs) and predict future HIV incidences. In Section 5, we summarize our results.

2. HIV epidemic game theory model

We employ an evolutionary game theory framework to model the decisions of individuals within a population about PrEP adoption. We denote the proportion of PrEP users at time t by $x(t)$. The evolution of their behavior can be described by the following differential equation:

$$x'(t) = x(1-x)(f_A - f_B),$$

where f_A is the fitness (relative success) of taking PrEP and f_B is the fitness of not taking it. In simple terms, the differential equation models the evolution of the proportion of individuals taking PrEP based on the relative fitness of taking PrEP compared to not taking it. The term $x(1-x)$ represents the interaction between two groups in the population: Those who take PrEP and those who do not. This term captures the fact that the change in $x(t)$ depends on the interaction between these two groups. The term $(f_A - f_B)$ represents the fitness advantage of taking PrEP compared to not taking it. If taking PrEP has a fitness advantage ($f_A > f_B$), then more people will adopt the behavior of taking PrEP. However, if not taking PrEP is more advantageous ($f_B > f_A$) and individuals are less likely to take PrEP, then the proportion of individuals taking PrEP will decrease over time. We assume that individuals are more likely to take PrEP as the number of HIV diagnoses increases and the awareness campaigns for PrEP intensify. We set $f_A = c_0\left(\left(q\beta\frac{I}{N} + q\beta_d\frac{T}{N}\right)P + \rho I\right) + \xi$, where the term $\left(q\beta\frac{I}{N} + q\beta_d\frac{T}{N}\right)P + \rho I$ denotes HIV diagnoses, and ξ denotes the intensity of PrEP awareness campaigns. However, people are less likely to take PrEP due to its side effects and stigma. Therefore, we set $f_B = \delta_0 x + r_S$, where r_S represents the side effects of PrEP, and the term $\delta_0 x$ denotes the stigma of taking PrEP. Here, we assume that the stigma associated with taking PrEP grows as PrEP uptake increases, reflecting the idea that greater prevalence of use raises broader awareness of the medication within the population. We define the behavior model of taking PrEP with the following differential equation.

$$x'(t) = x(1-x)\left(\underbrace{c_0\left(\left(q\beta\frac{I}{N} + q\beta_d\frac{T}{N}\right)P + \rho I\right) + \xi}_{f_A} - \underbrace{(\delta_0 x + r_S)}_{f_B}\right). \tag{2.1}$$

The behavior equation is of generalized logistic type. Because it is coupled to the epidemic model, its long-term behavior depends on the dynamics of the full system and is analyzed in Section 2.1.2.

We next model the population involved in the HIV epidemic transmission process using five compartments: Individuals susceptible to HIV (S), that is, individual at-risk, individuals observing

protective measures (P), individuals infected with HIV (I), individuals who are diagnosed and treated (T), and individuals with AIDS (A). Susceptible individuals are recruited at a rate of $\Lambda(1-x)$, where the recruitment represents individuals entering sexual activity, $(1-x)$ represents the proportion of individuals not using PrEP and therefore remain susceptible to infection. They can also become infected through contact with infected or treated individuals, with transmission rates β and β_d, respectively. Additionally, susceptible individuals can transition into the protected group due to the effect of PrEP at a rate ψ, or through other protective measures at a rate σ. The change in the protected population depends on the recruitment of individuals using PrEP Λx and their exposure to infection from infected and treated individuals at rates $q\beta$ and $q\beta_d$, respectively. Protected individuals can transition back to the susceptible group due to factors such as PrEP discontinuation and other dynamics, with transition rates ω and χ. Infected individuals can move into the treatment or AIDS compartments at rates ρ and γ, respectively. Treated individuals can transition to the AIDS class due to disease progression or resistance to medicines at a rate γ_d. Finally, individuals in all compartments, susceptible, protected, infected, treated, and those with AIDS, leave the system due to natural death at a rate μ. The total population size, N, is given by $N = S + P + I + T$, representing all individuals in the system except those who have progressed to AIDS.

$$
\begin{aligned}
\frac{d}{dt}S(t) &= \Lambda(1-x) - \beta\frac{SI}{N} - \beta_d\frac{ST}{N} + (\omega(1-x)+\chi)P - (\psi x + \sigma + \mu)S,\\
\frac{d}{dt}P(t) &= \Lambda x - q\beta\frac{PI}{N} - q\beta_d\frac{PT}{N} + (\psi x + \sigma)S - (\mu + \omega(1-x) + \chi)P,\\
\frac{d}{dt}I(t) &= \beta\frac{SI}{N} + \beta_d\frac{ST}{N} - (\rho + \gamma + \mu)I,\\
\frac{d}{dt}T(t) &= q\beta\frac{PI}{N} + q\beta_d\frac{PT}{N} + \rho I - (\gamma_d + \mu)T,\\
\frac{d}{dt}A(t) &= \gamma I + \gamma_d T - (\mu + \alpha)A.
\end{aligned}
\tag{2.2}
$$

A schematic representation of the interaction between the behavioral and epidemic models is given in Figure 1. The state variables and their definitions are presented in Table 1, and the model parameters are summarized in Table 2.

Table 1. State variables and their definitions.

State variable	Definition	Units
$S(t)$	Number of individuals susceptible to HIV at time t	Individuals
$P(t)$	Number of individuals observing protective measures at time t	Individuals
$I(t)$	Number of individuals infected with HIV at time t	Individuals
$T(t)$	Number of diagnosed and treated individuals at time t	Individuals
$A(t)$	Number of individuals with AIDS at time t	Individuals
$N(t)$	The total population, excluding those with AIDS at time t	Individuals
$x(t)$	Proportion of individuals who are taking PrEP at time t	–

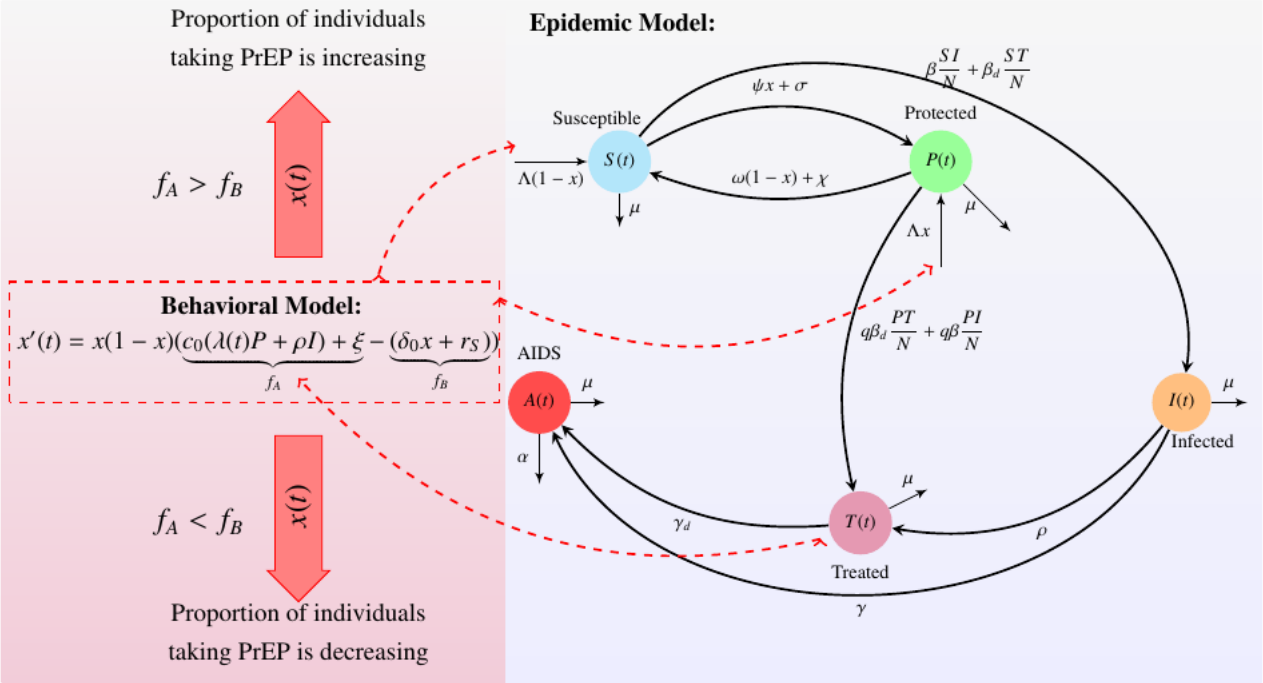

Figure 1. Flowchart: The interaction between behavioral and epidemic models in disease transmission. The red dash arrows represent the bidirectional relationship, where individual behaviors affect disease spread, and the epidemic influences behaviors. The epidemic-to-behavior link connects disease treatment and diagnosis to the effectiveness of taking PrEP, while the behavior-to-epidemic link shows how changes in PrEP uptake impact the recruitment rate of susceptible and protective individuals.

Table 2. Parameters and their definitions.

	Parameter	Definition	Units
Epidemic	Λ	Per capita recruitment rate of new susceptible and protected individuals	year^{-1}
	β	Infection rate of susceptible individuals from contact with infected individuals	year^{-1}
	β_d	Infection rate of susceptible individuals from contact with treated individuals	year^{-1}
	ω	Transition rate from protected to susceptible state due to PrEP discontinuation	year^{-1}
	χ	Transition rate from protected to susceptible state due to discontinuation of other protections	year^{-1}
	ψ	Transition rate from susceptible to protected state due to PrEP	year^{-1}
	σ	Transition rate from susceptible to protected state due to other protective measures	year^{-1}
	μ	Natural death rate of individuals in the population	year^{-1}
	q	Reduction factor for infection risk in protected individuals	–
	ρ	Treatment rate from the infected state to the treated state	year^{-1}
	γ	Progression rate from the infected state to the AIDS state	year^{-1}
	γ_d	Progression rate from the treated state to the AIDS state	year^{-1}
	α	Disease-induced death rate	year^{-1}
Behavioral	$\lambda(t)$	$= q\beta\frac{I}{N} + q\beta_d\frac{T}{N}$	
	ξ	Intensity of PrEP awareness campaigns	year^{-1}
	r_s	Side effects of PrEP	year^{-1}
	c_0, δ_0	Scaling coefficients	

2.1. Analysis of HIV epidemic behavior model

2.1.1. Equilibria and stability of the model without protection and PrEP

We will analyze the HIV epidemic and behavior model in two steps. PrEP was introduced in 2012 [28]; vaccines have been studied since the 1980s [29], and other protective measures, such as the Syringe exchange programs (SEPs) to combat HIV, have been recommended since the 1980s [30]. As a first step, we will consider the model without PrEP and protection classes. The model without protection and PrEP describes disease transmission among susceptible, infected, treated, and AIDS compartments, without considering interventions that reduce susceptibility. The model focuses on how the infection spreads and progresses without these preventive measures. The model is based on natural disease progression and infection dynamics and is given below:

$$\begin{aligned}
\frac{d}{dt}S(t) &= \Lambda - \beta\frac{SI}{N} - \beta_d\frac{ST}{N} - \mu S,\\
\frac{d}{dt}I(t) &= \beta\frac{SI}{N} + \beta_d\frac{ST}{N} - (\rho+\gamma+\mu)I,\\
\frac{d}{dt}T(t) &= \rho I - (\gamma_d+\mu)T,\\
\frac{d}{dt}A(t) &= \gamma I + \gamma_d T - (\mu+\alpha)A.
\end{aligned} \tag{2.3}$$

We first analyze the stability of the disease-free equilibrium, which refers to the state in which no HIV infection exists within the population. In our case, this means $S(t) > 0, I(t) = T(t) = A(t) = 0$. To determine the disease-free equilibrium E_0 for model (2.3), we set the right-hand side of system (2.3) to zero and obtain,

$$E_0 = \left\{\frac{\Lambda}{\mu}, 0, 0, 0\right\}.$$

The total population size at the disease-free equilibrium is given by, $N = S + I + T = \dfrac{\Lambda}{\mu}$. We present the stability result of the disease-free equilibrium in Theorem 2.1. The proof is provided in the Appendix.

Theorem 2.1. *The disease-free equilibrium E_0 is locally asymptotically stable if $\mathcal{R}_0 < 1$, and it is unstable if $\mathcal{R}_0 > 1$. $\mathcal{R}_0$ is given by*

$$\mathcal{R}_0 = \frac{\beta}{(\rho+\gamma+\mu)} + \frac{\beta_d\rho}{(\rho+\gamma+\mu)(\gamma_d+\mu)}.$$

In epidemiology, the reproduction number represents the average number of secondary cases an infectious individual produces in an entirely susceptible population. The first term of $\mathcal{R}_0$ accounts for the number of secondary infections generated by individuals in the infected class I. The incidence of new infections caused by these individuals is given by $\dfrac{\beta SI}{N}$, while their average duration in the infectious stage is $\dfrac{1}{\rho+\gamma+\mu}$, representing the time before progression to AIDS, treatment, or death. Thus, the total number of new infections produced by a single infected individual ($I = 1, \dfrac{S}{N} = 1$) is given by $\dfrac{\beta}{\rho+\gamma+\mu}$.

The second term of $\mathcal{R}_0$ represents the number of secondary infections produced by individuals in the treated class T in relation to disease transmission. The incidence of new infections caused by treated individuals is given by $\frac{\beta_d S T}{N}$. The fraction of individuals transitioning from I to T is $\frac{\rho}{\rho+\gamma+\mu}$, and the time spent in the treated class before progression to AIDS or death is $\frac{1}{\gamma_d+\mu}$. Together, these terms represent the expected number of secondary infections that a treated individual will generate during their infectious period.

We next establish results concerning the uniqueness and stability of the endemic equilibrium, with proofs given in the Appendix. The endemic equilibrium refers to the state in which the disease is present in the population. This implies that $S^* > 0, I^* > 0, T^* > 0$ and $A^* > 0$.

Theorem 2.2. *A unique endemic equilibrium E_1 of the system* (2.3) *exists when $\mathcal{R}_0 > 1$.*

Theorem 2.3. *Assume $\mathcal{R}_0 > 1$ and $\beta \geq \beta_d$. Then the endemic equilibrium E_1 in* (2.3) *is locally asymptotically stable.*

2.1.2. Equilibria and stability of HIV epidemic behavior model

As a second step, we analyze the full HIV model with behavior, incorporating PrEP and protection classes. The model given by Eqs (2.1) and (2.2) does not have a unique disease-free equilibrium. Instead, it has three distinct disease-free equilibria, determined by the behavioral state variable x. At each disease-free equilibrium, $I = T = A = 0$.

Equilibrium 1: $E_1^0 = (0, S_1^0, P_1^0, 0, 0, 0)$: Occurs when $x = 0$, representing a scenario where no individuals engage in PrEP or protection strategies.

Equilibrium 2: $E_2^0 = (1, S_2^0, P_2^0, 0, 0, 0)$,: Occurs when $x = 1$, representing a scenario where all individuals engage in PrEP or protection strategies.

Equilibrium 3: $E_3^0 = (x^*, S_3^0, P_3^0, 0, 0, 0)$: Represents an intermediate level of PrEP and protection uptake.

To determine these equilibria, we set the left-hand side of systems (2.1) and (2.2) to zero:

$$\begin{aligned}
0 &= x(1-x)\left(c_0\left(\left(q\beta\frac{I}{N} + q\beta_d\frac{T}{N}\right)P + \rho I\right) + \xi - (\delta_0 x + r_S)\right),\\
0 &= \Lambda(1-x) - \beta\frac{SI}{N} - \beta_d\frac{ST}{N} + (\omega(1-x)+\chi)P - (\psi x + \sigma + \mu)S,\\
0 &= \Lambda x - q\beta\frac{PI}{N} - q\beta_d\frac{PT}{N} + (\psi x + \sigma)S - (\mu + \omega(1-x) + \chi)P,\\
0 &= \beta\frac{SI}{N} + \beta_d\frac{ST}{N} - (\rho+\gamma+\mu)I,\\
0 &= q\beta\frac{PI}{N} + q\beta_d\frac{PT}{N} + \rho I - (\gamma_d+\mu)T,\\
0 &= \gamma I + \gamma_d T - (\mu+\alpha)A.
\end{aligned} \tag{2.4}$$

From the first equation of the system, we derive three possible solutions for x; $x = 0$, $x = 1$, and $x = x^*$, where $x^* = \frac{\xi - r_s}{\delta_0}$ exists if and only if $0 < \frac{\xi - r_S}{\delta_0} < 1$. Considering each of these solutions separately, we evaluate the resulting equilibrium points. When $x = 0$, solving for S from the third equation of

system (2.4), we obtain

$$S = \frac{(\mu + \omega + \chi)P}{\sigma}.$$

Next, we substitute S into the second equation of system (2.4) and solve for P and obtain

$$P = \frac{\Lambda\sigma}{\mu(\omega + \chi + \sigma + \mu)}.$$

Substituting this expression for P back into the equation for S, we get

$$S = \frac{\Lambda(\mu + \omega + \chi)}{\mu(\omega + \chi + \sigma + \mu)}.$$

Thus,

$$S_1^0 = \frac{\Lambda(\omega + \chi + \mu)}{\mu(\omega + \chi + \sigma + \mu)},$$

$$P_1^0 = \frac{\Lambda\sigma}{\mu(\omega + \chi + \sigma + \mu)}.$$

Since $N = S + P + I + T$,

$$N_1^0 = \frac{\Lambda}{\mu}.$$

When $x = 1$, using similar calculations, we obtain

$$S_2^0 = \frac{\Lambda\chi}{\mu(\psi + \sigma + \chi + \mu)},$$

$$P_2^0 = \frac{\Lambda(\psi + \sigma + \mu)}{\mu(\psi + \sigma + \chi + \mu)},$$

$$N_2^0 = \frac{\Lambda}{\mu}.$$

When $x = x^*$, using similar calculations, we obtain the following corresponding equilibrium values for S and P:

$$S_3^0 = \frac{\Lambda(1 - x^*)(\omega(1 - x^*) + \chi + \mu) + \Lambda x^*(\omega(1 - x^*) + \chi)}{\mu(\psi x^* + \sigma + \omega(1 - x^*) + \chi + \mu)}$$

$$P_3^0 = \frac{\Lambda(x^*\mu + \psi x^* + \sigma)}{\mu(\psi x^* + \sigma + \omega(1 - x^*) + \chi + \mu)}$$

$$N_3^0 = \frac{\Lambda}{\mu}.$$

The stability of the three disease-free equilibria is determined from the Jacobian matrix of the systems (2.1) and (2.2) at the disease-free equilibrium E_0 is

$$J(E_0) = \begin{bmatrix} (f_A - f_B)(1 - 2x) - \delta_0 x(1 - x) & 0 & 0 & x(1 - x)(c_0 q\beta p + c_0\rho) & x(1 - x)c_0 q\beta_d p & 0 \\ -\Lambda - \psi S - \omega P & -(\psi x + \sigma + \mu) & \omega(1 - x) + \chi & -\beta s & -\beta_d s & 0 \\ \Lambda + \psi S + \omega P & \psi x + \sigma & -(\omega(1 - x) + \chi + \mu) & -q\beta p & -q\beta_d p & 0 \\ 0 & 0 & 0 & \beta s - (\mu + \gamma + \rho) & \beta_d s & 0 \\ 0 & 0 & 0 & q\beta p + \rho & q\beta_d p - (\mu + \gamma_d) & 0 \\ 0 & 0 & 0 & \gamma & \gamma_d & -\mu - \alpha \end{bmatrix}.$$

Equilibrium 1: when $x = 0$;

Theorem 2.4. *The disease-free equilibrium E_1^0 is locally asymptotically stable if $\mathcal{R}_1 < 1$ and $\xi - r_s < 0$, and it is unstable if either inequality or both are reversed. $\mathcal{R}_1$ is given by,*

$$\mathcal{R}_1 = \frac{\beta(\omega+\chi+\mu)}{(\mu+\gamma+\rho)(\omega+\chi+\sigma+\mu)} + \frac{q\beta_d\sigma}{(\mu+\gamma_d)(\omega+\chi+\sigma+\mu)} + \frac{\rho\beta_d(\omega+\chi+\mu)}{(\mu+\gamma+\rho)(\mu+\gamma_d)(\omega+\chi+\sigma+\mu)}.$$

Proof. The Jacobian at the disease-free equilibrium E_1^0 is given by

$$J(E_1^0) = \begin{bmatrix} \xi - r_s & 0 & 0 & 0 & 0 & 0 \\ -\Lambda - \psi S_1^0 - \omega P_1^0 & -(\sigma+\mu) & \omega+\chi & -\beta s & -\beta_d s & 0 \\ \Lambda + \psi S_1^0 + \omega P_1^0 & \sigma & -(\omega+\chi+\mu) & -q\beta p & -q\beta_d p & 0 \\ 0 & 0 & 0 & \beta s - (\mu+\gamma+\rho) & \beta_d s & 0 \\ 0 & 0 & 0 & q\beta p + \rho & q\beta_d p - (\mu+\gamma_d) & 0 \\ 0 & 0 & 0 & \gamma & \gamma_d & -\mu-\alpha \end{bmatrix}.$$

Thus, one eigenvalue of the system is $-\mu-\alpha < 0$. Another eigenvalue of the system is $\xi - r_s$, and we assume $\xi - r_s < 0$. To demonstrate that the remaining eigenvalues have negative real parts, we analyze the following Jacobian matrix:

$$J(E_1^0)' = \begin{bmatrix} -(\sigma+\mu) & \omega+\chi & -\beta s & -\beta_d s \\ \sigma & -(\omega+\chi+\mu) & -q\beta p & -q\beta_d p \\ 0 & 0 & \beta s - (\mu+\gamma+\rho) & \beta_d s \\ 0 & 0 & q\beta p + \rho & q\beta_d p - (\mu+\gamma_d) \end{bmatrix} = \begin{bmatrix} A_{11} & A_{12} \\ A_{21} & A_{22} \end{bmatrix},$$

where $A_{11} = \begin{bmatrix} -(\sigma+\mu) & \omega+\chi \\ \sigma & -(\omega+\chi+\mu) \end{bmatrix}$ and $A_{22} = \begin{bmatrix} \beta s - (\mu+\gamma+\rho) & \beta_d s \\ q\beta p + \rho & q\beta_d p - (\mu+\gamma_d) \end{bmatrix}$.

Since matrix A_{21} is the zero matrix, its eigenvalues are exactly the eigenvalues of A_{11} and A_{22}. The eigenvalues of A_{11} are negative or with negative real parts since the trace of A_{11} is given by

$$Tr(A_{11}) = -(\sigma+\mu) - (\omega+\chi+\mu) < 0$$

and the determinant of A_{11} is

$$Det(A_{11}) = (\sigma+\mu)(\omega+\chi+\mu) - \sigma(\omega+\chi) = \mu(\sigma+\omega+\chi+\mu) > 0.$$

Thus, the trace and determinant confirm that the eigenvalues of A_{11} are negative or have negative real parts. As a result, the stability of the disease-free equilibrium depends on the eigenvalues of A_{22}. To show that the remaining eigenvalues of the system have negative real parts, we need to prove that the determinant of A_{22} is greater than zero and the trace of A_{22} is less than zero. Consider the following condition for the determinant of A_{22}:

$$Det(A_{22}) = (\beta s - (\mu+\gamma+\rho))(q\beta_d p - (\mu+\gamma_d)) - (q\beta p + \rho)(\beta_d s) > 0.$$

This leads to the inequality

$$\beta s(\mu+\gamma_d) + q\beta_d p(\mu+\gamma+\rho) + \rho\beta_d s < (\mu+\gamma+\rho)(\mu+\gamma_d).$$

This inequality defines a reproduction number as

$$\mathcal{R}_1 = \frac{\beta s}{(\mu+\gamma+\rho)} + q\frac{\beta_d p}{(\mu+\gamma_d)} + \rho\frac{\beta_d s}{(\mu+\gamma+\rho)(\mu+\gamma_d)},$$

which implies that

$$\mathcal{R}_1 = \frac{\beta(\omega+\chi+\mu)}{(\mu+\gamma+\rho)(\omega+\chi+\sigma+\mu)} + \frac{q\beta_d\sigma}{(\mu+\gamma_d)(\omega+\chi+\sigma+\mu)} + \frac{\rho\beta_d(\omega+\chi+\mu)}{(\mu+\gamma+\rho)(\mu+\gamma_d)(\omega+\chi+\sigma+\mu)}.$$

If $\mathcal{R}_1 < 1$, then $Det(A_{22}) > 0$ and

$$Tr(A_{22}) = \beta s - (\mu+\gamma+\rho) + q\beta_d p - (\mu+\gamma_d) < 0,$$

since $\mathcal{R}_1 < 1$ implies $\dfrac{\beta s}{\mu+\gamma+\rho} < 1$ and $\dfrac{q\beta_d p}{\mu+\gamma_d} < 1$.

Thus, the disease-free equilibrium E_1^0 is locally asymptotically stable if $\mathcal{R}_1 < 1$ and $\xi - r_s < 0$. On the other hand, if $\mathcal{R}_1 > 1$ or $\xi > r_S$, then there is a positive eigenvalue, and DFE E_1^0 is unstable. □

These results indicate that when $R_1 < 1$ and $\xi - r_s < 0$ the negative side effects outweigh the awareness campaign, and the reproduction number is less than one (each person infects less than one other person on average). In this case, any small increase in infections remains small.

The reproduction number can be interpreted in the following manner: The first term represents the number of non-PrEP users that one untreated infected individual infects; the second represents the number of PrEP user that one individual on treatment infects; and the third represents the number of non-Prep users that one individual on treatment infects. The reproduction number from 2.5 and 2.6 can be interpreted in a similar manner.

Equilibrium 2: when $x = 1$;

Theorem 2.5. *The disease-free equilibrium E_2^0 is locally asymptotically stable if $\mathcal{R}_2 < 1$ and $\xi-\delta_0-r_s > 0$, and it is unstable if either inequality or both are reversed. $\mathcal{R}_2$ is given by*

$$\mathcal{R}_2 = \frac{\beta\chi}{(\mu+\gamma+\rho)(\psi+\sigma+\chi+\mu)} + \frac{q\beta_d(\psi+\sigma+\mu)}{(\mu+\gamma_d)(\psi+\sigma+\chi+\mu)} + \frac{\rho\beta_d\chi}{(\mu+\gamma+\rho)(\mu+\gamma_d)(\psi+\sigma+\chi+\mu)}.$$

Proof. The Jacobian at the disease-free equilibrium E_2^0 is given by

$$J(E_2^0) = \begin{bmatrix} -(\xi-\delta_0-r_s) & 0 & 0 & 0 & 0 & 0 \\ -\Lambda-\psi S_2^0-\omega P_2^0 & -(\psi+\sigma+\mu) & \chi & -\beta s & -\beta_d s & 0 \\ \Lambda+\psi S_2^0+\omega P_2^0 & \psi+\mu & -(\chi+\mu) & -q\beta p & -q\beta_d p & 0 \\ 0 & 0 & 0 & \beta s-(\mu+\gamma+\rho) & \beta_d s & 0 \\ 0 & 0 & 0 & q\beta p+\rho & q\beta_d p-(\mu+\gamma_d) & 0 \\ 0 & 0 & 0 & \gamma & \gamma_d & -\mu-\alpha \end{bmatrix}.$$

Thus, one eigenvalue of the system is $-\mu-\alpha < 0$. Another eigenvalue of the system is $-(\xi-\delta_0-r_s)$, and we assume $\xi-\delta_0-r_s > 0$. To show that the remaining eigenvalues have negative real parts, we analyze the following Jacobian matrix:

$$J(E_2^0)' = \begin{bmatrix} -(\psi+\sigma+\mu) & \chi & -\beta s & -\beta_d s \\ \psi+\mu & -(\chi+\mu) & -q\beta p & -q\beta_d p \\ 0 & 0 & \beta s-(\mu+\gamma+\rho) & \beta_d s \\ 0 & 0 & q\beta p+\rho & q\beta_d p-(\mu+\gamma_d) \end{bmatrix} = \begin{bmatrix} B_{11} & B_{12} \\ B_{21} & B_{22} \end{bmatrix},$$

where $B_{11} = \begin{bmatrix} -(\psi+\sigma+\mu) & \chi \\ \psi+\mu & -(\chi+\mu) \end{bmatrix}$ and $B_{22} = \begin{bmatrix} \beta s - (\mu+\gamma+\rho) & \beta_d s \\ q\beta p + \rho & q\beta_d p - (\mu+\gamma_d) \end{bmatrix}$.

Since B_{21} is a zero matrix, the eigenvalues of the system are the same as the eigenvalues of B_{11} and B_{22}. The eigenvalues of B_{11} are negative or have negative real part, as indicated by the negative trace and positive determinant of B_{11}. Following the same computation in matrix B_{22} as before, we obtain an expression for the reproduction number $\mathcal{R}_2$:

$$\mathcal{R}_2 = \frac{\beta\chi}{(\mu+\gamma+\rho)(\psi+\sigma+\chi+\mu)} + \frac{q\beta_d(\psi+\sigma+\mu)}{(\mu+\gamma_d)(\psi+\sigma+\chi+\mu)} + \frac{\rho\beta_d\chi}{(\mu+\gamma+\rho)(\mu+\gamma_d)(\psi+\sigma+\chi+\mu)}.$$

If $\mathcal{R}_2 < 1$, then $Det(B_{22}) > 0$, and applying the same method as before, we can show that $Tr(B_{22}) < 0$. Therefore, the disease-free equilibrium E_2^0 is locally asymptotically stable if $\mathcal{R}_2 < 1$ and $\xi - \delta_0 - r_s > 0$. If, on the other hand, $\mathcal{R}_2 > 1$ or $\xi - \delta_0 - r_s < 0$, then there is a positive eigenvalue, and E_2^0 is unstable. □

Thus, when $R_2 < 1$ and $\xi - r_s < 0$, we have the negative side effects outweigh the awareness campaign, and the reproduction number is less than one (each person infects less than one other person on average). In this case, any small increase in infections remains small.

Equilibrium 3: when $x = x^*$;

Theorem 2.6. *The disease-free equilibrium E_3^0 is locally asymptotically stable if $\mathcal{R}_3 < 1$. If $\mathcal{R}_3 > 1$, E_3^0 is unstable. $\mathcal{R}_3$ is given by*

$$\mathcal{R}_3 = \frac{\beta(\omega(1-x^*)+\chi+(1-x^*)\mu)}{(\mu+\gamma+\rho)(\psi x^*+\sigma+\omega(1-x^*)+\chi+\mu)} + \frac{q\beta_d(\psi x^*+\sigma+x^*\mu)}{(\mu+\gamma_d)(\psi x^*+\sigma+\omega(1-x^*)+\chi+\mu)} + \frac{\rho\beta_d(\omega(1-x^*)+\chi+(1-x^*)\mu)}{(\mu+\gamma+\rho)(\mu+\gamma_d)(\psi x^*+\sigma+\omega(1-x^*)+\chi+\mu)}. \tag{2.5}$$

Proof. The Jacobian at the disease-free equilibrium E_3^0 is given by

$$J(E_3^0) = \begin{bmatrix} (f_A-f_B)(1-2x^*)-\delta_0 x^*(1-x^*) & 0 & 0 & x^*(1-x^*)(c_0q\beta p+c_0\rho) & x^*(1-x^*)c_0q\beta_d p & 0 \\ -\Lambda-\psi S-\omega P & -(\psi x^*+\sigma+\mu) & \omega(1-x^*)+\chi & -\beta s & -\beta_d s & 0 \\ \Lambda+\psi S+\omega P & \psi x^*+\sigma & -(\omega(1-x^*)+\chi+\mu) & -q\beta p & -q\beta_d p & 0 \\ 0 & 0 & 0 & \beta s-(\mu+\gamma+\rho) & \beta_d s & 0 \\ 0 & 0 & 0 & q\beta p+\rho & q\beta_d p-(\mu+\gamma_d) & 0 \\ 0 & 0 & 0 & \gamma & \gamma_d & -\mu-\alpha \end{bmatrix}.$$

Thus, one eigenvalue of the system is $-\mu - \alpha < 0$. The remaining eigenvalues are determined by the following matrix:

$$\begin{bmatrix} (f_A-f_B)(1-2x^*)-\delta_0 x^*(1-x^*) & 0 & 0 & x^*(1-x^*)(c_0q\beta p+c_0\rho) & x^*(1-x^*)c_0q\beta_d p \\ -\Lambda-\psi S-\omega P & -(\psi x^*+\sigma+\mu) & \omega(1-x^*)+\chi & -\beta s & -\beta_d s \\ \Lambda+\psi S+\omega P & \psi x^*+\sigma & -(\omega(1-x^*)+\chi+\mu) & -q\beta p & -q\beta_d p \\ 0 & 0 & 0 & \beta s-(\mu+\gamma+\rho) & \beta_d s \\ 0 & 0 & 0 & q\beta p+\rho & q\beta_d p-(\mu+\gamma_d) \end{bmatrix} = \begin{bmatrix} C_{11} & C_{12} \\ C_{21} & C_{22} \end{bmatrix},$$

where C_{11} is a 3×3 matrix, C_{22} is a 2×2 matrix, and C_{21} is a zero matrix. Therefore, the eigenvalues of the system are exactly the eigenvalues of C_{11} and C_{22}.

Using similar calculations for the C_{22} matrix as before, we can show that the following is an expression for the reproduction number $\mathcal{R}_3$:

$$\mathcal{R}_3 = \frac{\beta(\omega(1-x^*)+\chi+(1-x^*)\mu)}{(\mu+\gamma+\rho)(\psi x^*+\sigma+\omega(1-x^*)+\chi+\mu)} + \frac{q\beta_d(\psi x^*+\sigma+x^*\mu)}{(\mu+\gamma_d)(\psi x^*+\sigma+\omega(1-x^*)+\chi+\mu)} + \frac{\rho\beta_d(\omega(1-x^*)+\chi+(1-x^*)\mu)}{(\mu+\gamma+\rho)(\mu+\gamma_d)(\psi x^*+\sigma+\omega(1-x^*)+\chi+\mu)}.$$

To demonstrate that the remaining eigenvalues have negative real parts, we consider C_{11}, where

$$|C_{11}-rI| = \begin{bmatrix} (f_A-f_B)(1-2x^*)-\delta_0 x^*(1-x^*)-r & 0 & 0 \\ -\Lambda-\psi S-\omega P & -(\psi x^*+\sigma+\mu)-r & \omega(1-x^*)+\chi \\ \Lambda+\psi S+\omega P & \psi x^*+\sigma & -(\omega(1-x^*)+\chi+\mu)-r \end{bmatrix}.$$

Adding the second row to the third row, we have

$$|C_{11}-rI| = \begin{bmatrix} (f_A-f_B)(1-2x^*)-\delta_0 x^*(1-x^*)-r & 0 & 0 \\ -\Lambda-\psi S-\omega P & -(\psi x^*+\sigma+\mu)-r & \omega(1-x^*)+\chi \\ 0 & -\mu-\lambda & -\mu-r \end{bmatrix}.$$

Thus, $r = (f_A-f_B)(1-2x^*)-\delta_0 x^*(1-x^*) = -\delta_0 x^*(1-x^*)+(\xi-\delta_0 x^*-r_s)(1-2x^*) = -\delta_0 x^*(1-x^*) < 0$ is an eigenvalue of C_{11}. The remaining eigenvalues are $r = -\mu < 0$ and $r = -(\psi x^*+\sigma+\mu)-\omega(1-x^*)-\chi < 0$. Therefore, all eigenvalues have negative real parts, and E_3^0 is locally asymptotically stable. If, on the other hand, $\mathcal{R}_3 > 1$, then the Jacobian has a positive eigenvalue, and E_3^0 is unstable. □

We next examine conditions for the existence of endemic equilibria.

Theorem 2.7. *Suppose that $x^* = 0$. When $\mathcal{R}_1 > 1$, there is a single endemic equilibrium. Let*

$$a = \frac{q}{\rho+\gamma+\mu}\frac{\gamma_d+\mu+\rho}{\gamma_d+\mu},$$

$$c = (\mu+w+\chi+\sigma)(1-\mathcal{R}_1)$$

and

$$D_1 = q + \frac{\mu+\omega+\chi}{\rho+\gamma+\mu} + \frac{q(\rho+\gamma+\mu)\sigma+\rho(\mu+\omega+\chi)}{(\gamma_d+\mu)(\rho+\gamma+\mu)} - \frac{\beta q}{\rho+\gamma+\mu} - \frac{\beta_d\rho q}{(\gamma_d+\mu)(\rho+\gamma+\mu)}.$$

When $\mathcal{R}_1 < 1$, either $D_1 < 0$, and $D_1^2 - 4ac > 0$ and there are two endemic equilibria, or $D_1 > 0$, or $D_1^2 - 4ac < 0$ and there are no endemic equilibria.

Proof. Let $\lambda = \frac{\beta I+\beta_d T}{N}$. When $x^* = 0$, and we have a nontrivial equilibrium, we obtain

$$S = \frac{\Lambda(q\lambda+\mu+\omega+\chi)}{\lambda(q\lambda+\mu+\omega+\chi)-(\omega+\chi)\sigma+(\sigma+\mu)(q\lambda+\mu+\omega+\chi)},$$

$$P = \frac{\sigma S}{q\lambda+\mu+\omega+\chi},$$

$$I = \frac{\lambda S}{\rho+\gamma+\mu},$$

$$T = \frac{q\lambda P + \rho I}{(\gamma_d + \mu)}.$$

We use the fact that $\lambda N = \beta I + \beta_d T$ to get

$$\lambda(S + \frac{\sigma S}{(q\lambda + \mu + \omega + \chi)} + \frac{\lambda S}{(\rho + \gamma + \mu)} + \frac{q\lambda(\rho + \gamma + \mu)\sigma S + \rho\lambda(q\lambda + \mu + \omega + \chi)S}{(q\lambda + \mu + \omega + \chi)(\gamma_d + \mu)(\rho + \gamma + \mu)}) =$$

$$\frac{\beta\lambda S}{(\rho + \gamma + \mu)} + \frac{\beta_d(q\lambda(\rho + \gamma + \mu)\sigma S + \rho\lambda(q\lambda + \mu + \omega + \chi))S}{(q\lambda + \mu + \omega + \chi)(\gamma_d + \mu)(\rho + \gamma + \mu)}.$$

Multiplying both sides by $\frac{q\lambda+\mu+\omega+\chi}{\lambda S}$ gives us

$$(q\lambda + \mu + \omega + \chi) + \sigma + \frac{\lambda(q\lambda + \mu + \omega + \chi)}{(\rho + \gamma + \mu)} + \frac{(q\lambda(\rho + \gamma + \mu)\sigma + \rho\lambda(q\lambda + \mu + \omega + \chi))}{(\gamma_d + \mu)(\rho + \gamma + \mu)} =$$

$$\frac{\beta(q\lambda + \mu + \omega + \chi)}{(\rho + \gamma + \mu)} + \frac{\beta_d(q(\rho + \gamma + \mu)\sigma + \rho(q\lambda + \mu + \omega + \chi))}{(\gamma_d + \mu)(\rho + \gamma + \mu)}.$$

We set

$$f_1(\lambda) = q\lambda + \mu + \omega + \chi + \sigma + \frac{\lambda(q\lambda + \mu + \omega + \chi)}{(\rho + \gamma + \mu)} + \frac{(q\lambda(\rho + \gamma + \mu)\sigma + \rho\lambda(q\lambda + \mu + \omega + \chi))}{(\gamma_d + \mu)(\rho + \gamma + \mu)} -$$

$$\frac{\beta(q\lambda + \mu + \omega + \chi)}{(\rho + \gamma + \mu)} - \frac{\beta_d(q(\rho + \gamma + \mu)\sigma + \rho(q\lambda + \mu + \omega + \chi))}{(\gamma_d + \mu)(\rho + \gamma + \mu)}.$$

Any positive solution to equation $f_1(\lambda) = 0$ is also an endemic equilibrium. Since f_1 is a quadratic with a positive leading coefficient a, f_1 has one positive root if and only if its constant term, $f_1(0)$, is negative. We see that

$$f_1(0) = \mu + \omega + \chi + \sigma - \frac{\beta(\mu + \omega + \chi)}{(\rho + \gamma + \mu)} - \frac{\beta_d(q(\rho + \gamma + \mu)\sigma + \rho(\mu + \omega + \chi))}{(\gamma_d + \mu)(\rho + \gamma + \mu)}$$

$$= (\mu + \omega + \chi + \sigma)(1 - \mathcal{R}_1) =: c.$$

Thus, there is a single endemic equilibrium when $\mathcal{R}_1 > 1$. On the other hand, when $\mathcal{R}_1 < 1$, the number of solutions depends on the linear term D_1 and the discriminant $D_1^2 - 4ac$. If $D_1 > 0$, then there are no solutions. If $D_1 < 0$ and $D_1^2 - 4ac > 0$, then there are two solutions. □

Theorem 2.8. *Suppose that $x^* = 1$. When $\mathcal{R}_2 > 1$, there is a single endemic equilibrium. Let*

$$a_2 = \frac{q}{\gamma_d + \mu}$$

$$c_2 = (\chi + \psi + \sigma + \mu)(1 - \mathcal{R}_2)$$

and

$$D_2 = 1 + \frac{\chi}{(\rho + \gamma + \mu)} + \frac{q(\rho + \gamma + \mu)(\psi + \sigma + \mu) + \rho\chi}{(\rho + \gamma + \mu)(\gamma_d + \mu)} - \frac{\beta_d q}{(\gamma_d + \mu)}.$$

When $\mathcal{R}_2 < 1$, either $D_2 < 0$ and $D_2^2 - 4a_2c_2 > 0$, so there are two endemic equilibria, or $D_2 > 0$ or $D_2^2 - 4a_2c_2 < 0$, and there are no endemic equilibria.

Proof. When $x^* = 1$, and we have a nontrivial equilibrium, we obtain

$$P = \frac{\Lambda(\lambda+\psi+\sigma+\mu)}{q\lambda(\lambda+\psi+\sigma+\mu)-(\psi+\sigma)\chi+(\mu+\chi)(\lambda+\psi+\sigma+\mu)},$$

$$S = \frac{\chi P}{(\lambda+\psi+\sigma+\mu)},$$

$$I = \frac{\lambda S}{\rho+\gamma+\mu},$$

$$T = \frac{q\lambda P+\rho I}{(\gamma_d+\mu)}.$$

Then using $\lambda N = \beta I + \beta_d T$ gives us

$$\lambda\left(\frac{\chi P}{\lambda+\psi+\sigma+\mu} + P + \frac{\lambda\chi P}{(\rho+\gamma+\mu)(\lambda+\psi+\sigma+\mu)} + \frac{q\lambda(\rho+\gamma+\mu)(\lambda+\psi+\sigma+\mu)P+\rho\lambda\chi P}{(\rho+\gamma+\mu)(\lambda+\psi+\sigma+\mu)(\gamma_d+\mu)}\right)$$

$$= \frac{\beta\lambda\chi P}{(\rho+\gamma+\mu)(\lambda+\psi+\sigma+\mu)} + \frac{\beta_d(q\lambda(\rho+\gamma+\mu)(\lambda+\psi+\sigma+\mu)P+\rho\lambda\chi P)}{(\rho+\gamma+\mu)(\lambda+\psi+\sigma+\mu)(\gamma_d+\mu)}.$$

Multiplying both sides by $\frac{\lambda+\psi+\sigma+\mu}{\lambda P}$ gives

$$\chi + (\lambda+\psi+\sigma+\mu) + \frac{\lambda\chi}{(\rho+\gamma+\mu)} + \frac{q\lambda(\rho+\gamma+\mu)(\lambda+\psi+\sigma+\mu)+\rho\lambda\chi}{(\rho+\gamma+\mu)(\gamma_d+\mu)} =$$

$$\frac{\beta\chi}{(\rho+\gamma+\mu)} + \frac{\beta_d(q(\rho+\gamma+\mu)(\lambda+\psi+\sigma+\mu)+\rho\chi)}{(\rho+\gamma+\mu)(\gamma_d+\mu)}.$$

Let

$$f_2(\lambda) = \chi + (\lambda+\psi+\sigma+\mu) + \frac{\lambda\chi}{(\rho+\gamma+\mu)} + \frac{q\lambda(\rho+\gamma+\mu)(\lambda+\psi+\sigma+\mu)+\rho\lambda\chi}{(\rho+\gamma+\mu)(\gamma_d+\mu)} -$$

$$\frac{\beta\chi}{(\rho+\gamma+\mu)} - \frac{\beta_d(q(\rho+\gamma+\mu)(\lambda+\psi+\sigma+\mu)+\rho\chi)}{(\rho+\gamma+\mu)(\gamma_d+\mu)}.$$

Then we get that

$$f_2(0) = \chi+\psi+\sigma+\mu - \frac{\beta\chi}{(\rho+\gamma+\mu)} - \frac{\beta_d(q(\rho+\gamma+\mu)(\psi+\sigma+\mu)+\rho\chi)}{(\rho+\gamma+\mu)(\gamma_d+\mu)}$$

$$= \chi+\psi+\sigma+\mu(1-\mathcal{R}_2).$$

Since the linear term of f_2 is D_2 and the discriminant is $D_2^2 - 4a_2c_2$, we get the desired result using the same reasoning as in (2.7). □

Figure 2 illustrates the backward bifurcation and the presence of multiple equilibria for the cases $x = 0$ and $x = 1$.

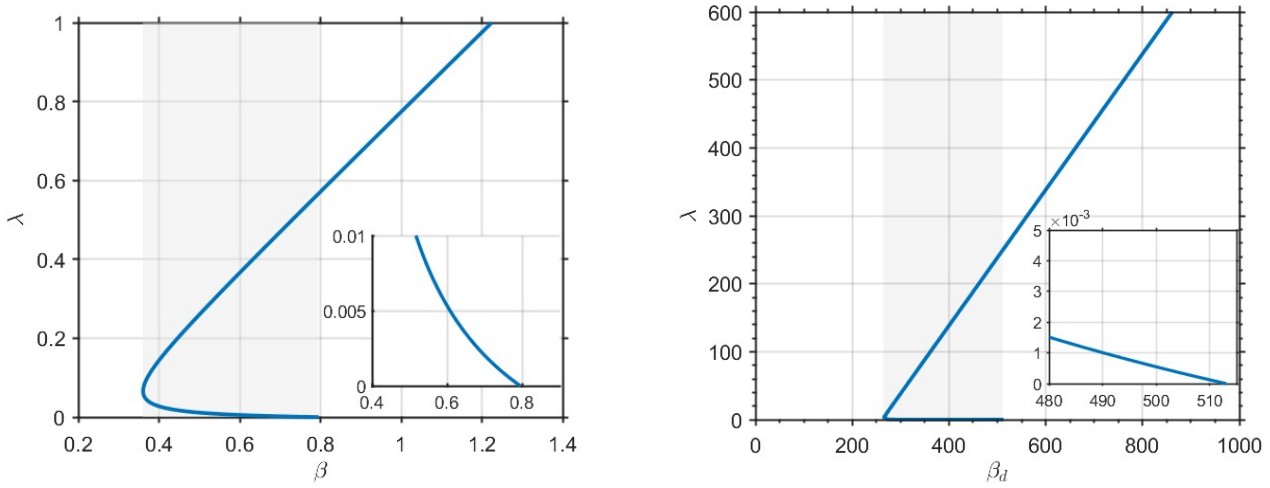

(a) $x = 0$ **(b)** $x = 1$

Figure 2. Bifurcation diagrams show the force of infection λ in terms of (a) the transmission rate β from infected individuals when $x = 0$, and (b) the transmission rate β_d from treated individuals when $x = 1$. The shaded region indicates the parameter range in which two endemic equilibria coexist, corresponding to a backward bifurcation. The insets provide a magnified view near the backward bifurcation point, illustrating the two branches of endemic equilibria emerging as the bifurcation parameter crosses its critical threshold.

Theorem 2.9. *Suppose that* $0 < x^* < 1$. *Then there exists an interior endemic equilibrium if the following conditions are satisfied:*

1) $0 < \frac{\xi - r_S}{\delta_0} < 1$.

2) $\bar{q}\Lambda c_0 - q(\delta_0 + r_S - \xi) < 0$, *where* $\bar{q} = \max\{q, \frac{\rho}{\rho+\gamma+\mu}\}$.

3) $\mathcal{R}_3 > 1$ *where* $\mathcal{R}_3$ *is defined in* (2.5).

Proof. Here, we are looking for an endemic equilibrium for which x^* is strictly between zero and one. We let

$$\lambda = \frac{\beta I}{N} + \frac{\beta_d T}{N}.$$

Using this notation, from the first two equations of (2.4), we get S and P in terms of λ and x:

$$S = \frac{\Lambda(1-x)(q\lambda + \mu + w(1-x) + \chi) + \Lambda x(w(1-x) + \chi)}{(\lambda + \psi x + \sigma + \mu)(q\lambda + \mu + w(1-x) + \chi) - (w(1-x) + \chi)(\psi x + \sigma)}, \tag{2.6}$$

$$P = \frac{\Lambda(1-x)(\psi x + \sigma) + \Lambda x(\lambda + \psi x + \sigma + \mu)}{(\lambda + \psi x + \sigma + \mu)(q\lambda + \mu + w(1-x) + \chi) - (w(1-x) + \chi)(\psi x + \sigma)}. \tag{2.7}$$

From the equation for x, we have

$$q\lambda P + \rho I = \frac{\delta_0 x + r_S - \xi}{c_0}. \tag{2.8}$$

From the equation for I, we have

$$I = \frac{\lambda S}{\rho + \gamma + \mu}. \tag{2.9}$$

Changing P and S in (2.8), we get the following equation for x and λ

$$q\lambda\frac{\Lambda(1-x)(\psi x+\sigma)+\Lambda x(\lambda+\psi x+\sigma+\mu)}{(\lambda+\psi x+\sigma+\mu)(q\lambda+\mu+w(1-x)+\chi)-(w(1-x)+\chi)(\psi x+\sigma)}$$
$$+\frac{\rho\lambda}{\rho+\gamma+\mu}\frac{\Lambda(1-x)(q\lambda+\mu+w(1-x)+\chi)+\Lambda x(w(1-x)+\chi)}{(\lambda+\psi x+\sigma+\mu)(q\lambda+\mu+w(1-x)+\chi)-(w(1-x)+\chi)(\psi x+\sigma)}=\frac{\delta_0 x+r_S-\xi}{c_0}. \tag{2.10}$$

We rewrite this equation as $f(x)=0$, where

$$f(x)=q\lambda\frac{\Lambda(1-x)(\psi x+\sigma)+\Lambda x(\lambda+\psi x+\sigma+\mu)}{(\lambda+\psi x+\sigma+\mu)(q\lambda+\mu+w(1-x)+\chi)-(w(1-x)+\chi)(\psi x+\sigma)}$$
$$+\frac{\rho\lambda}{\rho+\gamma+\mu}\frac{\Lambda(1-x)(q\lambda+\mu+w(1-x)+\chi)+\Lambda x(w(1-x)+\chi)}{(\lambda+\psi x+\sigma+\mu)(q\lambda+\mu+w(1-x)+\chi)-(w(1-x)+\chi)(\psi x+\sigma)}-\frac{\delta_0 x+r_S-\xi}{c_0}.$$

From (2.8), we see that we need

$$\frac{\delta_0 x+r_S-\xi}{c_0}>0.$$

Hence, we need $x>\frac{\xi-r_s}{\delta_0}$. Assume

$$0<\frac{\xi-r_s}{\delta_0}<1.$$

Then, we look for x such that

$$\frac{\xi-r_s}{\delta_0}<x<1.$$

It is not hard to see that for any $\lambda>0$, we have $f(\frac{\xi-r_s}{\delta_0})>0$. To show that $f(1)<0$, denote

$$\bar{q}=\max\{q,\frac{\rho}{\rho+\gamma+\mu}\}.$$

Then we have

$$\begin{aligned}
f(1)&=q\lambda\frac{\Lambda(\lambda+\psi+\sigma+\mu)}{(\lambda+\psi x+\sigma+\mu)(q\lambda+\mu+\chi)-\chi(\psi x+\sigma)}\\
&+\frac{\rho\lambda}{\rho+\gamma+\mu}\frac{\Lambda\chi}{(\lambda+\psi+\sigma+\mu)(q\lambda+\mu+\chi)-\chi(\psi x+\sigma)}-\frac{\delta_0+r_S-\xi}{c_0}\\
&\le\bar{q}\lambda\frac{\Lambda(\lambda+\psi+\sigma+\mu+\chi)}{(\lambda+\psi+\sigma+\mu+\chi)(q\lambda+\mu)}-\frac{\delta_0+r_S-\xi}{c_0}\\
&\le\frac{\bar{q}\Lambda\lambda}{q\lambda+\mu}-\frac{\delta_0+r_S-\xi}{c_0}\\
&\le\frac{\bar{q}\Lambda}{q}-\frac{\delta_0+r_S-\xi}{c_0}.
\end{aligned}$$

Assume

$$\frac{\bar{q}\Lambda}{q}-\frac{\delta_0+r_S-\xi}{c_0}<0,$$

where $\bar{q}=\max\{q,\frac{\rho}{\rho+\gamma+\mu}\}$. We note that from what we have assumed $\delta_0+r_S-\xi>0$, the above inequality is meaningful and can be satisfied. Because $f(\frac{\xi-r_S}{\delta_0})>0$, but $f(1)<0$ for any $\lambda>0$, we conclude that equation $f(x)=0$ has at least one solution for any $\lambda>0$. However, equation $f(x)=0$ can be rewritten

as a quadratic equation in x, and therefore has at most two solutions. However, since the number of solutions of $f(x) = 0$ must be odd, the equation has exactly one solution $x \in (\frac{\xi - r_S}{\delta_0}, 1)$ for every $\lambda > 0$. This solution defines x as a function of λ, $x = g(\lambda)$.

Next, we need to obtain an equation for λ. From the definition of λ, we have

$$\lambda = \frac{\beta I}{N} + \frac{\beta_d T}{N}.$$

We express I, T, and N in terms of S and P. From the equilibrium equation of the total population size, we have

$$N = \frac{\Lambda}{\mu} - \frac{\gamma}{\mu} I - \frac{\gamma_d}{\mu} T$$

$$= \frac{\Lambda}{\mu} - \frac{\gamma}{\mu} \frac{\lambda S}{\rho + \gamma + \mu} - \frac{\gamma_d}{\mu} \frac{1}{\gamma_d + \mu} \left(q\lambda P + \frac{\rho}{\rho + \gamma + \mu} \lambda S \right).$$

We rewrite the equation for λ in the form

$$\lambda N = \beta I + \frac{\beta_d}{\gamma_d + \mu} (q\lambda P + \rho I)$$

Replacing I with its expression in S, we have

$$\lambda N = \beta \frac{\lambda S}{\rho + \gamma + \mu} + \frac{\beta_d}{\gamma_d + \mu} (q\lambda P + \rho \frac{\lambda S}{\rho + \gamma + \mu}).$$

Canceling λ from both sides of the equation and collecting terms, we have the following equation for λ:

$$\frac{\Lambda}{\mu} - \frac{\gamma}{\mu} \frac{\lambda S}{\rho + \gamma + \mu} - \frac{\gamma_d}{\mu} \frac{1}{\gamma_d + \mu} \left(q\lambda P + \frac{\rho}{\rho + \gamma + \mu} \lambda S \right) = \left(\beta + \frac{\beta_d \rho}{\gamma_d + \mu} \right) \frac{S}{\rho + \gamma + \mu} + \frac{\beta_d q P}{\gamma_d + \mu}. \tag{2.11}$$

We recall that S and P are functions of λ. Denoting the LHS of (2.11) as $h_1(\lambda)$ and the RHS as $h_2(\lambda)$, we can rewrite Eq (2.11) as $h_1(\lambda) = h_2(\lambda)$. We first compare $h_1(0)$ with $h_2(0)$. We begin by computing $x_0 = g(0)$. Thus, we solve $f(x) = 0$ for $\lambda = 0$ and obtain

$$x_0 = \frac{\xi - r_S}{\delta_0}.$$

Thus, $h_1(0) = \frac{\Lambda}{\mu}$, so

$$h_2(0) = \left(\beta + \frac{\beta_d \rho}{\gamma_d + \mu} \right) \frac{S(x_0, 0)}{\rho + \gamma + \mu} + \frac{\beta_d q P(x_0, 0)}{\gamma_d + \mu}.$$

Define the reproduction number

$$\mathcal{R}_3 = \frac{\mu}{\Lambda} \left(\left(\beta + \frac{\beta_d \rho}{\gamma_d + \mu} \right) \frac{S(x_0, 0)}{\rho + \gamma + \mu} + \frac{\beta_d q P(x_0, 0)}{\gamma_d + \mu} \right).$$

We note that this is $\mathcal{R}_3$ also defined in (2.5). Assume $\mathcal{R}_3 > 1$. Then $h_1(0) < h_2(0)$.

Next, we compare the two sides of Eq (2.11) for $\lambda \to \infty$. First, we determine $x_\infty = \lim_{\lambda \to \infty} g(\lambda)$. Letting $\lambda \to \infty$ in $f(x) = 0$, we get the following equation for x_∞:

$$\frac{q\Lambda x}{q} + \frac{\rho}{\rho + \gamma + \mu} \frac{\Lambda q (1 - x)}{q} - \frac{\delta_0 x + r_S - \xi}{c_0} = 0.$$

Solving this equation for x, we obtain

$$x_\infty = \frac{\frac{\rho\Lambda}{\rho+\gamma+\mu} - \frac{r_S-\xi}{c_0}}{\frac{\delta_0}{c_0} - \Lambda\frac{\gamma+\mu}{\rho+\gamma+\mu}}.$$

According to our construction $x_\infty \in (\frac{\xi-r_S}{\delta_0}, 1)$, we consider (2.11) for $x = x_\infty$ and $\lambda \to \infty$. First, we notice that

$$\lim_{\lambda\to\infty} \lambda S = \frac{\Lambda q(1-x_\infty)}{q} \qquad \lim_{\lambda\to\infty} S = 0$$

$$\lim_{\lambda\to\infty} \lambda P = \frac{\Lambda x_\infty}{q} \qquad \lim_{\lambda\to\infty} P = 0.$$

From Eq (2.11), we have

$$h_1(\infty) - h_2(\infty) = \frac{\Lambda}{\mu} - \frac{\gamma}{\mu}\frac{1}{\rho+\gamma+\mu}\frac{\Lambda q(1-x_\infty)}{q} - \frac{\gamma_d}{\mu(\gamma_d+\mu)}\left(\frac{q\Lambda x_\infty}{q} + \frac{\rho}{\rho+\gamma+\mu}\frac{\Lambda q(1-x_\infty)}{q}\right)$$

$$\geq \frac{\Lambda}{\mu}\left(1 - \frac{\gamma}{\rho+\gamma+\mu}(1-x_\infty) - \frac{\gamma_d}{\gamma_d+\mu}x_\infty - \frac{\gamma_d}{\gamma_d+\mu}\frac{\rho}{\rho+\gamma+\mu}(1-x_\infty)\right)$$

$$\geq \left(1 - \frac{\gamma+\rho}{\rho+\gamma+\mu}(1-x_\infty) - \frac{\gamma_d}{\gamma_d+\mu}x_\infty\right) > 0.$$

Hence, $h_1(\infty) > h_2(\infty)$. Since, for $\lambda > 0$, h_1 and h_2 are continuous functions, there exists a $\lambda^* > 0$, such that it solves Eq (2.11). Further, $x^* = g(\lambda^*)$ solves $f(x^*) = 0$ and satisfies $x^* \in (\frac{\xi-r_S}{\delta_0}, 1)$. Substituting x^* and λ^* in the expressions for S, P, I, T, and A, we obtain an interior equilibrium of the system. This completes the proof. □

3. Course of the HIV epidemic in the United States

3.1. Data

In this study, we incorporated HIV incidence data from three sources. The first data set was obtained from a study published in the Morbidity and Mortality Weekly Report (MMWR), which estimated the annual number of HIV infections in the United States from 1981 to 2019 [31]. We applied mathematical modeling methods to data from the national HIV surveillance system, categorizing HIV incidence estimation into three distinct time periods. From 1981 to 2006, HIV incidence was estimated using an extended back-calculation approach based on HIV surveillance data. In 2007, a stratified extrapolation approach was applied to the CDC surveillance data to estimate the incidence. From 2008 to 2019, HIV incidence estimates were derived from the CDC report [31].

The second data set was obtained from CDC AtlasPlus, an online database that provides surveillance data on HIV incidence and other public health indicators in the United States [32]. AtlasPlus data used in this study covered HIV incidences from 2019 to 2022.

In addition to historical data, we included projected HIV incidence estimates for 2025 and 2030, based on the EHE initiative targets. The EHE initiative aims to reduce new HIV infections by 75% by 2025 and by 90% by 2030 [33]. All data used in this study, including historical estimates and projected values, are provided in Table 3.

Table 3. HIV incidence data from 1981 to 2022 and projected values for 2025 and 2030 (in thousands). Data from 1981 to 2019 is sourced from [31], while data from 2019 to 2022 is obtained from [32]. The years 2025 and 2030 are shown in bold to represent the goals of the initiative to reduce new HIV infections in the United States by 75% by 2025 and by at least 90% by 2030, with the aim of preventing 250,000 new HIV infections [33].

Year	Incidences (1000s)	Year	Incidences (1000s)	Year	Incidences (1000s)	Year	Incidences (1000s)
1981	20.82	1992	48.42	2003	55.45	2014	37.89
1982	65.48	1993	48.67	2004	55.20	2015	38.39
1983	65.23	1994	48.67	2005	55.20	2016	38.39
1984	130.47	1995	48.92	2006	55.70	2017	37.13
1985	130.47	1996	49.18	2007	53.44	2018	36.38
1986	85.56	1997	58.46	2008	41.65	2019	35.38
1987	85.30	1998	58.96	2009	40.65	2020	38.3
1988	84.80	1999	58.21	2010	39.64	2021	38.4
1989	84.30	2000	55.45	2011	38.89	2022	39.4
1990	84.55	2001	55.20	2012	38.39	**2025**	**9.3** (goal)
1991	48.67	2002	55.45	2013	37.63	**2030**	**3** (goal)

For the model with PrEP and protection, we also incorporated two more datasets: (i) PrEP usage data, representing the proportion of individuals on PrEP in the United States from 2015 to 2023 [32], with projections for 2025 and 2030 based on national goals [33]; and (ii) AIDS classifications data, reported annual AIDS classifications for the same period [32]. All data used, including historical and projected values, are summarized in Tables 4 and 5.

Table 4. Proportion of individuals on PrEP in the United States (2016–2023) with projections for 2025 and 2030. Data from 2016 to 2023 are obtained from [32].Projected values for 2025 and 2030 are shown in bold to reflect national goals to increase PrEP usage by 50% by those years [33].

Year	Proportion using PrEP
2016	0.07
2017	0.132
2018	0.182
2019	0.227
2020	0.248
2021	0.301
2022	0.36
2023	0.313
2025	**0.5** (goal)
2030	**0.5** (goal)

Table 5. AIDS classifications in the United States (2015–2023) sourced from [32].

Year	AIDS classifications (1000s)
2015	18.511
2016	18.265
2017	17.712
2018	17.080
2019	16.386
2020	14.350
2021	16.008
2022	16.731
2023	17.409

3.2. Structural identifiability analysis

Structural identifiability is a fundamental property that determines whether model parameters can be uniquely estimated from idealized, noise-free data. For formal definitions, we consider the following [34].

Definition 3.1. *Consider the model*

$$x'(t) = f(x, \mathbf{p}), \tag{3.1}$$

with observations

$$y(t) = g(x, \mathbf{p}),$$

where x denotes the state variables, $\mathbf{p}$ *the parameter vector, and y the measured output. The model is said to be globally (uniquely) structurally identifiable if*

$$g(x, \mathbf{p}) = g(x, \hat{\mathbf{p}}) \;\Rightarrow\; \mathbf{p} = \hat{\mathbf{p}}.$$

Definition 3.2. *The model* (3.1) *is locally structurally identifiable if, for any* $\mathbf{p}$ *in an open neighborhood of* $\hat{\mathbf{p}}$*,*

$$g(x, \mathbf{p}) = g(x, \hat{\mathbf{p}}) \;\Rightarrow\; \mathbf{p} = \hat{\mathbf{p}}.$$

In this study, we assessed structural identifiability using the *StructuralIdentifiability.jl* package in Julia [35]. Within this framework, a parameter was said to be locally identifiable if it could be recovered from the input–output time series up to a finite number of admissible values, whereas global identifiability corresponded to unique recovery. We performed the identifiability analysis for two models: The model without protection and PrEP, and the full epidemic-behavioral model.

3.2.1. Structural identifiability results of the model without protection and PrEP

For the model without protection and PrEP (2.3), the observed data included CDC estimated HIV incidences $y_1(t) = \beta\frac{SI}{N} + \beta_d\frac{ST}{N}$. The structural identifiability analysis was performed using the

StructuralIdentifiability.jl package in JULIA. The results indicated that parameters γ, Λ, β, and μ are globally structurally identifiable, while γ_d, ρ, and β_d are locally identifiable. However, α is not structurally identifiable from the observation $y_1(t)$. Therefore, model (2.3) is not structurally identifiable. We summarize these results in the following propostion.

Proposition 3.1. *The model without protection and PrEP, Eq* (2.3)*, with either unknown or known initial conditions, is not structurally identifiable for all its parameters from the observation of HIV incidences $y_1(t)$. Specifically, with unknown initial conditions, γ, Λ, β, and μ are globally structurally identifiable, γ_d, ρ, and β_d are locally structurally identifiable, while α remains unidentifiable. With known initial conditions, $\gamma, \Lambda, \beta, \gamma_d, \rho, \beta_d$, and μ are globally structurally identifiable, but α remains unidentifiable.*

A structurally unidentifiable model can be made identifiable by incorporating additional observations or fixing unidentifiable parameters. Based on the known correlations among identifiable parameter combinations (see Table 6), we fix α and ρ and repeat the identifiability analysis. The analysis confirms that the model becomes structurally identifiable when α and ρ are fixed. We note that alternative choices (e.g., fixing β_d or γ_d together with α) also lead to a structurally identifiable model. We chose to fix ρ because it is strongly correlated with β_d and γ_d.

Proposition 3.2. *The model without protection and PrEP, Eq* (2.3)*, with either unknown or known initial conditions, becomes structurally identifiable for all its parameters from the observation of HIV incidences $y_1(t)$, when α and ρ are fixed.*

3.2.2. Structural identifiability results of the model with PrEP

The structural identifiability analysis with PrEP involves an epidemic (2.2) and behavioral model (2.1), as PrEP introduces a behavioral component that influences the dynamics of the epidemic. The observations used in this analysis include CDC-estimated HIV incidences $y_1(t) = \beta\frac{SI}{N} + \beta_d\frac{ST}{N}$ and the proportion of individuals on PrEP $y_2(t) = x(t)$. Due to the complexity of the models, they cannot be fully executed in Julia when two observations were used. To address this issue, we added an additional observation: the number of AIDS classifications $y_3 = \gamma I + \gamma_d T$. The results indicated that the parameters α, ξ, and r_s are not structurally identifiable, while all other parameters are structurally identifiable with the three observations. As a result, we fix α and ξ or r_s to make the model structurally identifiable.

Proposition 3.3. *The model with PrEP, Eq* (2.2)*, with either unknown or known initial conditions, is not structurally identifiable for all its parameters from the observations of HIV incidence $y_1(t)$, the proportion of individuals in PrEP $y_2(t)$, and the number of AIDS classifications $y_3(t)$.*

Proposition 3.4. *The model with PrEP, Eq* (2.2)*, with either unknown or known initial conditions, becomes structurally identifiable for all its parameters from the observations of HIV incidence $y_1(t)$, the proportion of individuals in PrEP $y_2(t)$, and the number of AIDS classifications $y_3(t)$, when ξ and α or r_s and α are fixed.*

The results obtained from the StructuralIdentifiability.jl package in Julia are presented in Table 6.

Table 6. Structural identifiability results: Parameters are classified as globally identifiable, locally identifiable, or non-identifiable based on the results obtained using *StructuralIdentifiability.jl* in Julia. Identifiability is evaluated under different observation scenarios and assumptions regarding known and unknown initial conditions, with selected parameters fixed as needed to achieve structural identifiability. Rows 2 and 5 indicate the structurally identifiable configuration for each model.

Model	Observed States or Fixed Parameters	without IC	Correlations	with IC
Model 2.3	observed states: y_1	$\{\gamma, \Lambda, \beta, \mu\}$ globally identifiable $\{\gamma_d, \rho, \beta_d\}$ locally identifiable $\{\alpha\}$ nonidentifiable	$\gamma_d + \rho$, $\rho\beta - \rho\beta_d$, $\gamma\rho - \gamma_d\rho$	$\{\gamma, \Lambda, \beta, \mu, \gamma_d, \rho, \beta_d\}$ globally identifiable $\{\}$ locally identifiable $\{\alpha\}$ nonidentifiable
Model 2.3	observed states: y_1 fixed parameters: α, ρ	All parameters are globally identifiable	–	All parameters are globally identifiable
Model 2.2	observed states: y_1, y_2	No results obtained from Julia due to a memory error		No results obtained from Julia due to a memory error
Model 2.2	observed states: y_1, y_2, y_3	$\{\Lambda, \beta, \beta_d, c, \chi, \delta, \gamma, \gamma_d, \mu, \omega, \psi, q, \rho, \sigma\}$ globally identifiable $\{\xi, r_s, \alpha\}$ nonidentifiable	$\xi - r_s$	$\{\Lambda, \beta, \beta_d, c, \chi, \delta, \gamma, \gamma_d, \mu, \omega, \psi, q, \rho, \sigma\}$ globally identifiable $\{\xi, r_s, \alpha\}$ nonidentifiable
Model 2.2	observed states: y_1, y_2, y_3 fixed parameters: ξ and α or r_s and α	All parameters are globally identifiable	–	All parameters are globally identifiable

3.3. Fitting model to data

3.3.1. Fitting model 2.3: Model without protection and PrEP

After performing the structural identifiability analysis, we proceeded to data fitting. We first applied data fitting to the model without protection and PrEP classes. Two scenarios were considered: (i) Fitting the model using data from 1981 to 2019, where 2019 corresponded to the initiation of the EHE initiative, and (ii) fitting the model to the entire timeline, using data from 1981 to 2019 along with discrete data points from 2020, 2021, 2022, 2025, and 2030 to assess its predictive performance. The data points used in both cases are provided in Table 3.

We first fit the model to HIV incidence data from 1981 to 2019. As shown by the structural identifiability analysis, fixing the diagnosis rate ρ and the disease-induced death rate α is necessary to

ensure the structural identifiability of the model. Therefore, in this data fitting, we fixed $\rho = \frac{1}{3}$ and $\alpha = 0.6$ based on estimates indicating that the average time from HIV infection to diagnosis is approximately 3 years, and the average time from AIDS diagnosis to death is around 1.6 years [36]. Furthermore, we fixed μ to prevent it from being estimated at an unrealistically small value. Since μ represents the average sexually active lifetime, we set it at $\mu = 0.02$, which corresponds to a value of 50 years to ensure realistic modeling.

The initial conditions for the model were set as $\{S(0), I(0), T(0), A(0)\} = \{820, 42, 0, 0.337\}$, where $S(0)$ was pre-estimated and fixed during fitting, and the remaining values were taken from [37]. We estimated the parameter vector $\mathbf{p_1} = \{\Lambda, \beta, \beta_d, \gamma, \gamma_d\}$ of the model (2.3) by fitting it to HIV incidence data from 1981 to 2019. Parameter estimation was performed by minimizing the least-squares objective functional

$$LS(\mathbf{p_1}) = \sum_{i=1}^{n} (y_1^{model}(t_i, \mathbf{p_1}) - y_1^{data}(t_i))^2, \tag{3.2}$$

where $y_1^{\text{model}}(t_i, \mathbf{p_1})$ denotes the HIV incidence predicted by the model at time t_i, $y_1^{\text{data}}(t_i)$ denotes the observed HIV incidence at time t_i, and n is the total number of observations. The optimization problem was solved using MATLAB's fmincon function, incorporating lower and upper bounds on the fitted parameters. To ensure biological realism, we also implemented biological constraints in the optimization procedure, including $\beta_d \leq \beta$ and $\gamma_d \leq \gamma$, based on the assumptions that treated individuals had a lower transmission rate compared to untreated susceptible individuals and a slower disease progression rate compared to untreated infected individuals. The estimated values and the corresponding parameter bounds are provided in Table 7, and the fitting is presented in Figure 3.

Table 7. Parameter estimates for the model without protection and PrEP (Eq (2.3)) obtained by solving the least squares problem with $p = \{\Lambda, \beta, \beta_d, \gamma, \gamma_d\}$ using data from 1981–2019 provided in Table 3. The fixed parameters are $\rho = \frac{1}{3}$, $\alpha = 0.6$, and $\mu = 0.02$.

Parameter	Λ	β	β_d	γ	γ_d
Bounds	[0, 6000]	[0, inf]	[0, 10]	[0.02, 1]	[0.02, 0.5]
Value	49.5548	1.0851	0.1713	0.3628	0.0200

Next, we fit the model to the entire timeline, incorporating both historical HIV incidence data and projected estimates for 2025 and 2030, aligning with the goals of the EHE initiative. EHE, introduced in 2019 by the United States. Department of Health and Human Services, aims to reduce new HIV infections in the United States by 75% by 2025 and 90% by 2030. The initiative focuses on four major strategies: Early diagnosis of HIV, providing rapid and effective treatment to achieve viral suppression, expanding access to proven prevention methods such as PrEP, and responding quickly to emerging HIV outbreaks to prevent further transmission.

In the data fitting, all parameters remained constant until 2019. After 2019, three parameters, $\beta_d(t), \gamma_d(t)$, and $\rho(t)$, were modeled as time-dependent parameters and adjusted based on the objectives of the EHE initiative. The remaining parameters were fixed at the estimated values from the previous fitting, which are given in Table 7. A key objective of EHE is to increase viral suppression to 95% by 2025 in the United States through rapid and effective treatment. Since our model did not include a within-host compartment, this goal was achieved by modifying the epidemic

parameter $\beta_d(t)$, which represents the transmission rate (or infection rate) from treated individuals to susceptible individuals. To reflect the increasing effectiveness of treatment and viral suppression, $\beta_d(t)$ was set to decrease linearly over time. Furthermore, with improved treatment, individuals in the treated class remained there longer and were less likely to progress to AIDS. This corresponded to a reduction in $\gamma_d(t)$, the progression rate from the treated state to AIDS, which was modeled as decreasing linearly over time. Finally, a key objective of EHE was to accelerate diagnosis, ensuring that individuals entered the treated class more quickly. In the model, this translated to the diagnosis rate, $\rho(t)$, increasing linearly over time.

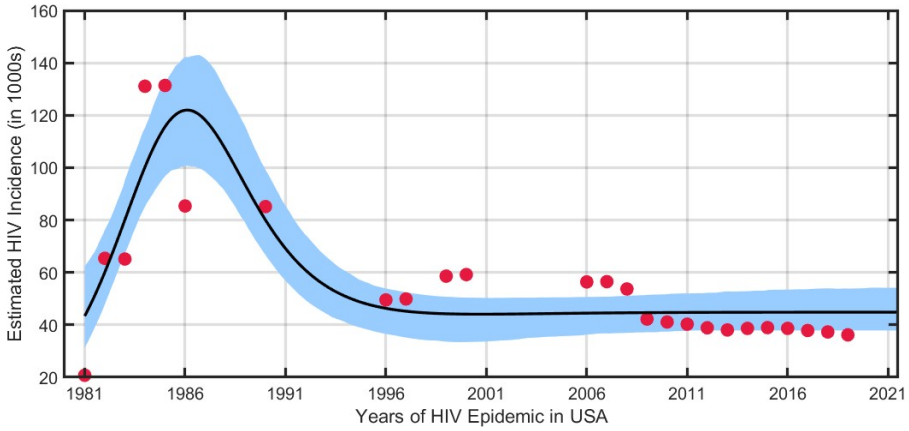

Figure 3. Observed HIV incidence data (red circles) plotted alongside the model prediction (black curve) of annual HIV infections in the United States from 1981 to 2019, generated by the fitted model (Eq (2.3)) using the estimated parameter set $\mathbf{p_1} = \{\Lambda, \beta, \beta_d, \gamma, \gamma_d\}$ in Table 7, and the fixed parameter set $\{\rho, \alpha, \mu\} = \{\frac{1}{3}, 0.6, 0.02\}$. The shaded blue region represents the 95% confidence interval derived from 1000 fitted trajectories to synthetic data, generated from normal distributions with means given by the model predictions and a specified standard deviation $\sigma = 15.1105$.

For $t > 38$ (where $t = 38$ corresponds to the year 2019), the time-dependent parameters are defined as

$$\beta_d(t) = -m_\beta(t - 38) + \beta_{d_{est}},$$

$$\gamma_d(t) = -m_\gamma(t - 38) + \gamma_{d_{est}},$$

$$\rho(t) = m_\rho(t - 38) + \rho_{fix},$$

Here, $\beta_{d_{est}}$ and $\gamma_{d_{est}}$ are the estimated values for β_d and γ_d (Table 7), while ρ_{fix} is the fixed value of ρ. The parameter (slope) vector $\mathbf{p_2} = \{m_\beta, m_\gamma, m_\rho\}$ is estimated using the fmincon function in MATLAB by minimizing the objective function Eq (3.2) used in the previous parameter estimation. The estimated values are reported in Table 8, with the corresponding time-dependent parameters shown in Figure 4. The corresponding model fit is presented in Figure 5.

Table 8. Estimated slopes of the time-dependent parameters $\beta_d(t)$, $\gamma_d(t)$, and $\rho(t)$ obtained by fitting the model to HIV incidence data from 1981 to 2019 and projected estimates for 2025 and 2030. For $t < 38$ (corresponding to years before 2019), all parameters are fixed to their estimated values given in Table 7, while for $t > 38$, $\beta_d(t)$, $\gamma_d(t)$, and $\rho(t)$ are adjusted.

Parameter	$\beta_d(t)$	$\gamma_d(t)$	$\rho(t)$
Slope	$m_\beta = 0.0154$	$m_\gamma = 2.4882 \times 10^{-5}$	$m_\rho = 0.2466$
Function	$-0.0154(t-38) + 0.1713$	$-2.4882 \times 10^{-5}(t-38) + 0.0200$	$0.2466(t-38) + \frac{1}{3}$

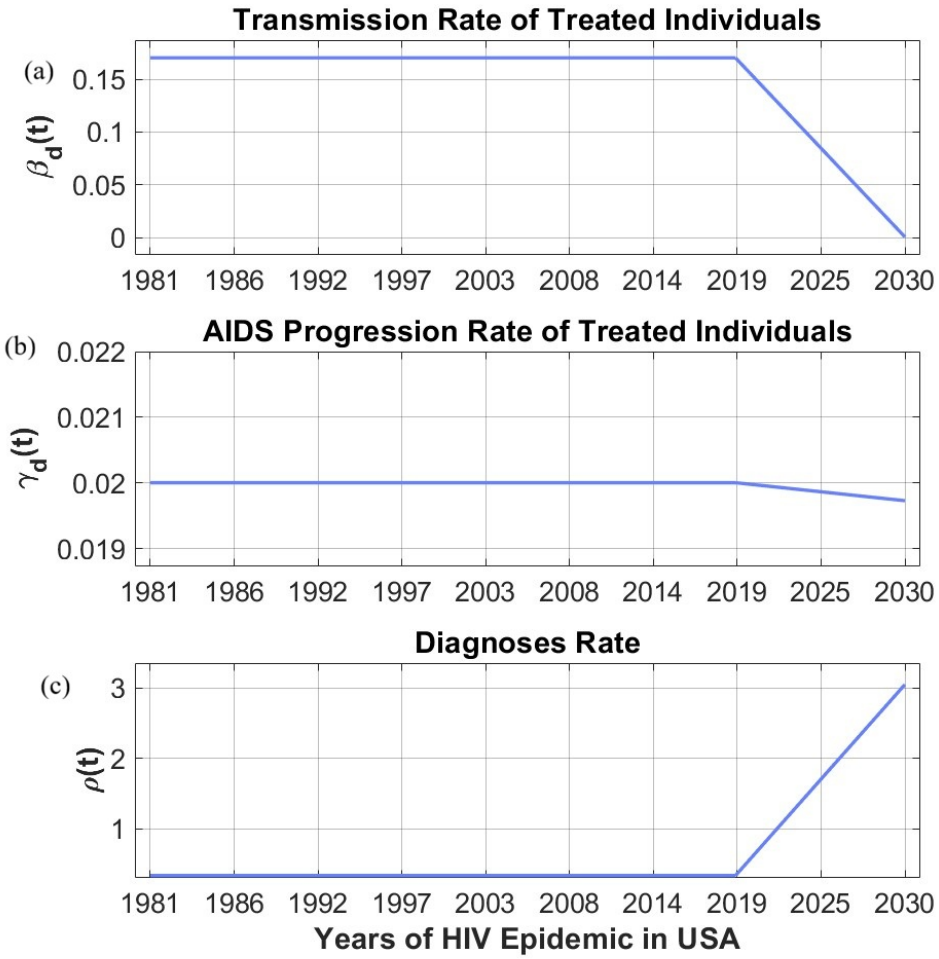

Figure 4. Time-varying parameters in the model (Eq (2.3)) in the United States from 1981 to 2030. (a) The transmission rate of treated individuals, $\beta_d(t)$, with a constant value for the first part of the epidemic and a linear decline thereafter. (b) The AIDS progression rate of treated individuals, $\gamma_d(t)$, following a similar pattern with a constant value until the transition at year 2019, after which it decreases linearly. (c) The diagnosis rate, $\rho(t)$, which remains constant initially and increases linearly after year 2019.

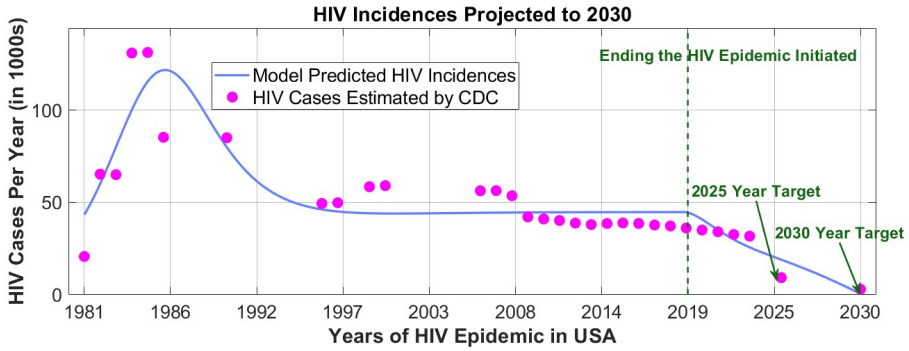

Figure 5. Projected and observed HIV incidences in the United States from 1981 to 2030. The solid blue line represents the model predictions of annual HIV incidences, while the magenta circles denote the observed and predicted HIV cases per year, as reported in Table 3. The vertical dashed line at 2019 marks the initiation of the EHE initiative. Arrows highlight the projected targets for 2025 and 2030.

3.3.2. Fitting model 2.2: Model with protection and PrEP

We next fit the extended model that incorporates behavioral dynamics through protection and PrEP usage. Model fitting began in 2015 due to the availability of PrEP-related data starting from that year, enabling accurate estimation of parameters related to protection and PrEP uptake. As in the previous case, we considered two fitting scenarios: (i) Fitting the model to data from 2015 to 2023, and (ii) fitting the model to the timeline data from 2015 to 2023, together with two projected discrete data points at 2025 and 2030. The initial conditions were used as $\{x(0), S(0), P(0), I(0), T(0), A(0)\} = \{0.0289515, 4000, 100, 200, 800, 12.779\}$. Three types of data were used for fitting: HIV incidence data, the proportion of the number of people in PrEP, and the number of AIDS classifications.

First, we fit the model to HIV incidence, PrEP usage, and AIDS classification data from 2015 to 2023. According to the structural identifiability analysis, fixing the parameters ξ and α, or r_s and α is required to ensure the structural identifiability of the model. Therefore, in this data fitting, we fixed $\xi - r_s$ (denoted as ξ_{r_s}) and α to $\xi_{r_s} = 0.8916$ and $\alpha = 230.62$. As in the previous section, we also fixed μ, retaining its value of $\mu = 0.02$ to ensure consistency with biologically realistic assumptions.

As in the previous section, parameter estimation was performed using ordinary least squares. Since the fitting procedure involved multiple data sets with different magnitudes, the weights ω_1 and ω_2 were introduced in the least squares objective to account for scale differences. The parameter vector $\mathbf{p_3} = \{\omega, \chi, \psi, \sigma, \rho, \gamma, \gamma_d, \beta, \beta_d, q, \Lambda\}$ was estimated by minimizing the weighted objective functional given by

$$LS(\mathbf{p_3}) = \omega_1 \sum_{i=1}^{n} (y_1^{model}(t_i, \mathbf{p_3}) - y_1^{data}(t_i))^2 + \sum_{j=1}^{m} (y_2^{model}(t_j, \mathbf{p_3}) - y_2^{data}(t_j))^2 + \omega_2 \sum_{k=1}^{l} (y_3^{model}(t_k, \mathbf{p_3}) - y_3^{data}(t_k))^2, \quad (3.3)$$

which incorporated three observed quantities. Here, y_1^{model}, y_2^{model}, and y_3^{model} denote the model-predicted HIV incidence, PrEP usage, and AIDS classifications, respectively, while y_1^{data}, y_2^{data}, and y_3^{data} represent the corresponding observed data. The weights were fixed at $\omega_1 = 0.01$ and $\omega_2 = 0.0001$ and n, m, and l represent the number of data points for the incidence, PrEP usage, and AIDS classification data sets, respectively.

The optimization problem was solved with MATLAB's *fmincon* algorithm, incorporating lower and upper bounds on the estimated parameters, along with the biological constraints $\beta_d \leq \beta$ and $\gamma_d \leq \gamma$. The estimated parameter values and their corresponding bounds are provided in Table 9, and the resulting model fits are presented in Figure 6.

Table 9. Parameter estimates for the model with protection and PrEP (Eq (2.2)) obtained by solving the least squares problem with $p = \{\omega, \chi, \psi, \sigma, \rho, \gamma, \gamma_d, \beta, \beta_d, q, \Lambda\}$, using data from 2015–2023 provided in Tables 3–5. The fixed parameters are $\mu = 0.02$, $\alpha = 230.62$, $c_0 = 0.0000001$, $\delta_0 = 2.6026$, and $\xi_{r_s} = 0.891575$.

Parameter	ω	χ	ψ	σ	ρ	γ
Bounds	$[0, 10^5]$	$[0, 10^5]$	$[0, 10^5]$	$[0, 10^5]$	$[0, 10^5]$	$[0, 10^5]$
Value	196.90	93.74	106.32	4.07	0.10	0.09
Parameter	γ_d	β	β_d	q	Λ	
Bounds	$[0, 10^5]$	$[0, 10^5]$	$[0, 10^5]$	$[0, 0.25]$	$[0, 10^7]$	
Value	0.0006	0.24	0.0011	0.08	675.10	

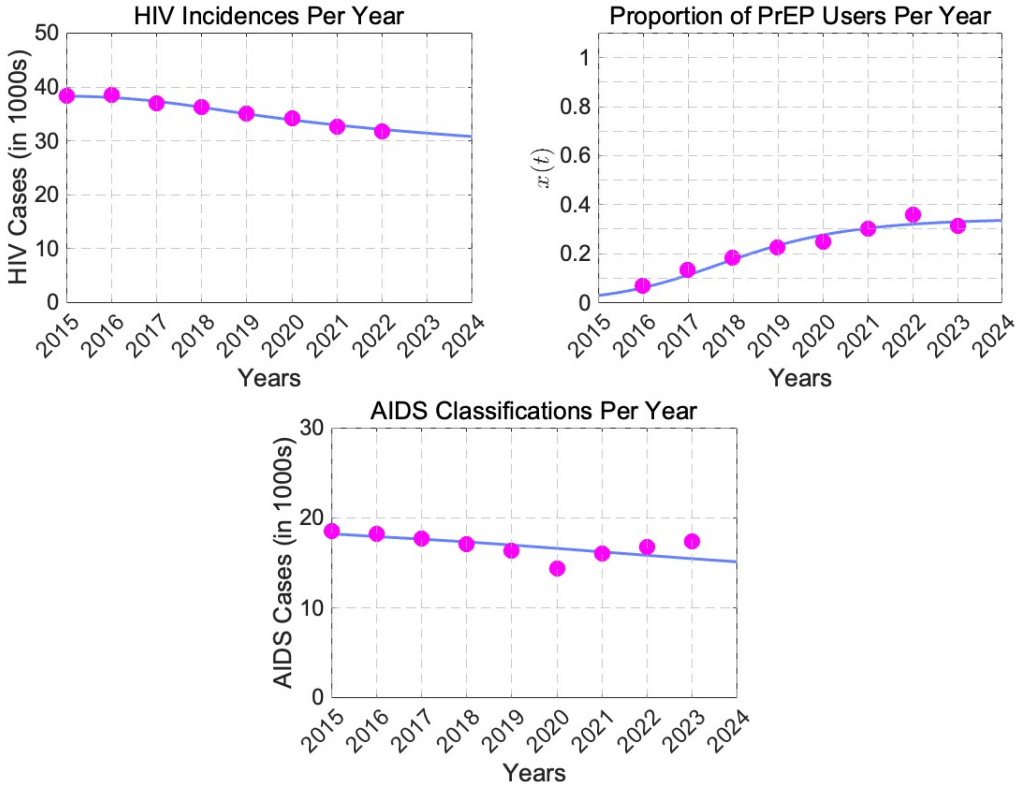

Figure 6. Observed HIV incidence data, the proportion of the number of people in PrEP, and the number of AIDS classifications (magenta circles) plotted alongside the model prediction (blue curves) from 2015 to 2023, generated by the fitted model (Eq (2.2)) using the estimated parameter set $\mathbf{p_3} = \{\omega, \chi, \psi, \sigma, \rho, \gamma, \gamma_d, \beta, \beta_d, q, \Lambda\}$ in Table 9, and the fixed parameter set $\{\mu, \alpha, c_0, \delta_0, \xi_{r_s}\} = \{0.02, 230.62, 0.0000001, 2.6026, 0.891575\}$.

Next, we fit the model to the timeline, incorporating historical data and projected estimates for 2025 and 2030, in alignment with the goals of the EHE initiative. The EHE aims to reduce new HIV infections in the United States by 75% by 2025 and 90% by 2030, while increasing PrEP coverage by 50% by 2030.

In the data fitting, all parameters were held constant through 2019. After 2019, the transmission rate $\beta_d(t)$ and $(\xi - r_s)(t)$ (denoted as $\xi_{r_s}(t)$) were modeled as time-dependent parameters and adjusted to reflect the objectives of the EHE initiative. Since the estimated value of β_d was extremely small, we set $\beta_d = 0$ in the post-2019 analysis and enabled only $\xi_{rs}(t)$ to vary linearly over time. The remaining parameters are fixed at the values estimated during the previous fitting, as provided in Table 9.

For $t > 8$ (where $t = 8$ corresponds to the year 2019), the time-dependent parameter is defined as,

$$\xi_{r_s}(t) = m_\xi(t - 8) + (\xi_{r_s})_{fix}.$$

Here, $(\xi_{r_s})_{fix}$ represents the fixed value of $\xi - r_s$. The slope parameter $\mathbf{p_4} = m_\xi$ was estimated using the MATLAB fmincon function by minimizing objective function Eq (3.3). The resulting parameter estimate is presented in Table 10, and the corresponding time-dependent parameter is shown in Figure 7. The fitting is shown in Figure 8.

Table 10. Estimated slope of time-dependent parameter $\xi_{rs}(t)$ obtained by fitting the model to data from 2015 to 2023, along with projected estimates for 2025 and 2030. For $t < 8$ (corresponding to years before 2019), all parameters are fixed at their estimated values given in Table 9. For $t \geq 8$, since the estimated value of β_d is extremely small, we set $\beta_d = 0$ and allow only $\xi_{rs}(t)$ to vary linearly over time, while the remaining parameters are kept fixed.

Parameter	$\xi_{r_s}(t)$
Slope	$m_\xi = 0.0978$
Function	$0.0978(t - 8) + 0.8916$

Next, we perform a sensitivity analysis to assess how variation in key parameters influences model behavior and epidemiological outcomes (see Figure 9).

Figure 9 demonstrates that the model exhibits markedly different sensitivity to c_0, δ_0, and $\xi - r_S$. Changes in c_0 (Figure 9(a)), which parameterizes the effect of HIV diagnoses on PrEP uptake, produce negligible differences in model trajectories across the full range of values examined. PrEP uptake increases steadily while incidence and diagnoses decline, and these patterns remain essentially unchanged regardless of c_0, indicating that diagnosis-driven behavioral feedback contributes little to population-level dynamics in this setting.

Parameter δ_0 (Figure 9(b)), representing the suppressive effect of social stigma, exerts a substantially larger influence across all modeled outcomes. Higher values of δ_0 markedly suppress uptake and yield more limited reductions in incidence and diagnoses, whereas lower values permit more rapid uptake expansion and produce considerably greater epidemiological improvements. The observed data are most consistent with intermediate-to-high values of δ_0, suggesting that stigma remains an important structural barrier to PrEP adoption in this population.

Parameter $\xi - r_S$ (Figure 9(c)), capturing the net balance between PrEP promotion and deterrence from perceived side effects, exerts comparably strong influence and exhibits threshold-dependent behavior. At low values, uptake remains minimal, and reductions in incidence and diagnoses are

correspondingly small; as $\xi - r_S$ increases, uptake accelerates, and beyond a critical range, the model yields substantial epidemiological improvements.

Overall, these results suggest that variation in stigma and net promotional effort drives most of the differences in model outcomes, while diagnosis-driven behavioral feedback plays a comparatively minor role.

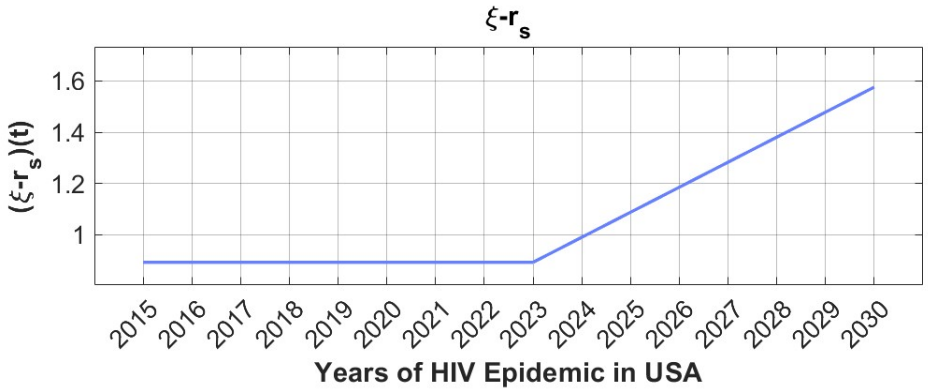

Figure 7. Time-varying parameter in the model (Eq (2.2)) for the United States from 2015 to 2030. All parameters are held constant before 2019. After 2019, since the estimated value of β_d is negligible, we set $\beta_d = 0$ and allow only $(\xi - r_s)(t)$ to vary linearly under the EHE initiative.

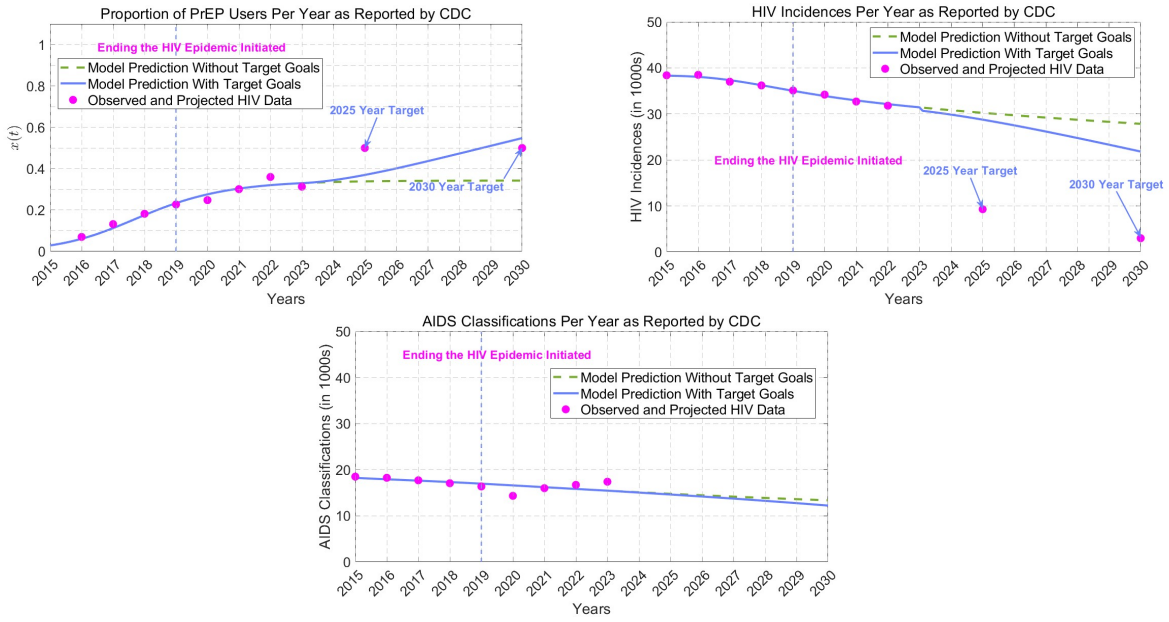

Figure 8. Projected and observed HIV incidences, PrEP coverage, and AIDS classifications in the United States from 2015 to 2030. The solid blue line represents the model predictions, while the magenta circles indicate observed and projected HIV data. The green dashed line shows the model prediction without incorporating EHE target goals. The vertical dashed line at 2019 marks the initiation of the EHE initiative.

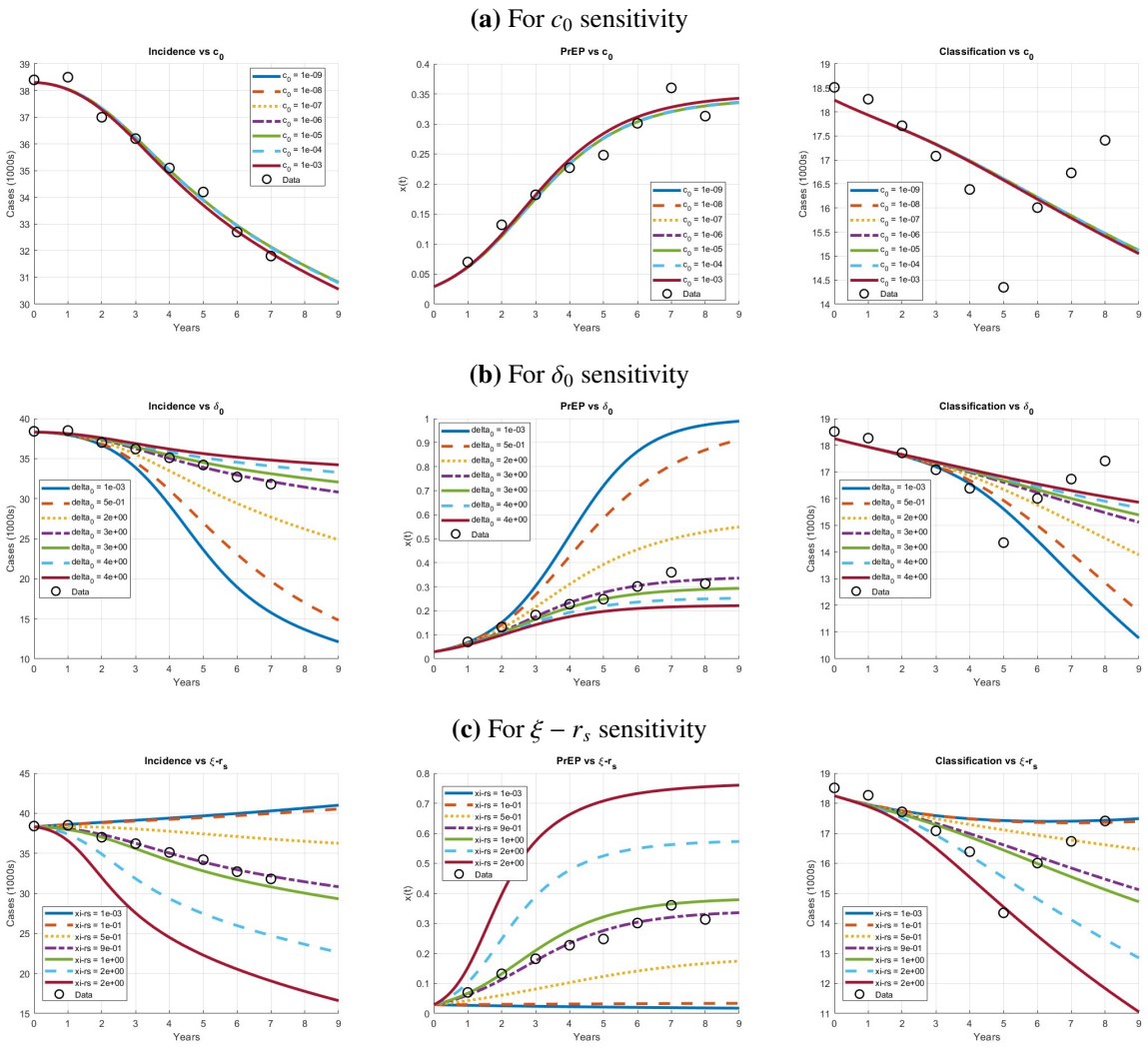

Figure 9. Sensitivity analysis of model outputs to key behavioral and social parameters, c_0, the strength with which HIV diagnoses influence the adoption of PrEP; δ_0, the strength of social stigma against using PrEP; and $\xi - r_S$, the net effect of promotion by doctors and media (ξ) relative to deterrence from PrEP side effects (r_S), over time (years). Rows correspond to variation in c_0 (panel a), δ_0 (panel b), and $\xi - r_S$ (panel c), while columns show (left to right) incidence, PrEP uptake $x(t)$, and AIDS classification outcomes. Colored curves represent model simulations under different parameter values, and open circles denote observed data.

4. Virtual epidemics

Epidemics rarely follow a single deterministic trajectory, as host responses, contact patterns, and environmental conditions vary substantially across populations and over time. Nevertheless, epidemiological models are often calibrated to a single dataset, yielding predictions that represent an average or nominal outbreak scenario. While surveillance data provide essential population-level information, they are frequently affected by underreporting, missing observations, testing constraints,

and reporting delays, all of which introduce uncertainty and can undermine parameter estimation and predictive accuracy. As a result, models calibrated to a single realization may fail to capture the breadth of plausible epidemic dynamics.

To address these challenges and more faithfully represent outbreak variability, we introduce the concept of VEs. Each VE corresponds to a plausible realization of disease spread that is consistent with known epidemiological dynamics and available data. By generating an ensemble of such epidemics, we can explicitly explore uncertainty in transmission dynamics, assess the robustness of model predictions, and evaluate the sensitivity of intervention outcomes to variation in model parameters.

In this section, we define VEs as distinct parameterizations of an epidemiological model that remain consistent with epidemiological observations. This framework is inspired by the well-established concept of virtual patients in systems pharmacology and computational biology, where individual-level model parameter sets are constrained by physiological and clinical data to represent inter-individual variability in disease progression and treatment response [38–40]. Collections of virtual patients form virtual populations, enabling uncertainty quantification, sensitivity analysis, and the evaluation of therapeutic strategies across heterogeneous populations. Analogously, VEs extend this paradigm to epidemics, capturing variability in transmission processes and behavioral responses that cannot be inferred from a single dataset alone. This approach provides a systematic framework for testing intervention strategies, quantifying uncertainty in epidemic projections, and assessing the stability of qualitative model conclusions under parameter uncertainty.

The construction of virtual patients typically involves formulating a mechanistic model, estimating parameters from experimental or clinical data, and identifying influential parameters through sensitivity or identifiability analyzes. Virtual patients may then be generated using one of two main approaches: (i) Sampling-based methods, in which parameters are drawn from prescribed distributions and retained if model outputs satisfy predefined acceptance criteria, or (ii) data-fitting methods, in which parameter sets arise from successful calibrations to observed data [39]. We adopted the data-fitting approach to generate an ensemble of VEs, ensuring consistency with observed epidemiological trends while preserving variability across plausible outbreak scenarios.

We present a workflow for generating VEs through identifiability-guided model calibration and data fitting. We outline a systematic framework for generating VEs that integrates epidemiological questions, mechanistic modeling, identifiability analysis, and data fitting to capture variability and uncertainty in disease dynamics. The flowchart in Figure 10 summarizes the workflow for generating VEs. Starting from an epidemiological question, a mathematical model was formulated and assessed for structural identifiability; if it failed, the model was revised by fixing parameters, rescaling, or incorporating additional data. Once structurally identifiable, the model was fitted to data and then evaluated for practical identifiability. When practical identifiability was achieved, an ensemble of parameter sets was used to create VEs, which collectively supported robust answers to the original epidemiological question by capturing uncertainty and variability in epidemic dynamics.

The epidemiological question we sought to address was whether it was possible to end the HIV epidemic in the United States. To this end, we developed two compartmental models that incorporated intervention strategies initiated under the EHE initiative. Both models were rendered structurally identifiable by fixing a subset of parameter values. The models were then calibrated using HIV surveillance data from the CDC. Prior to generating VEs, we conducted a practical identifiability analysis for both models. This analysis was performed using Monte Carlo-based simulations, with

methodological details provided in the Appendix. Using the definition in [34], we found that, for the model without PrEP, parameters Λ, β, β_d, and γ are strongly practically identifiable, whereas γ_d is weakly practically identifiable (see Table 11). In contrast, for the model with PrEP, weak practical identifiability was observed only for the parameters ω, χ, ψ, σ, γ, ρ, β, and Λ (see Table 12). All remaining parameters are practically unidentifiable, indicating that they cannot be reliably estimated from the available data. The identifiability analysis of the PrEP model indicates that some parameters are practically unidentifiable. Consequently, we did not generate VEs for this model, as parameter non-identifiability would undermine the reliability of the resulting epidemic projections. Such projections would therefore be inappropriate for addressing the epidemiological question.

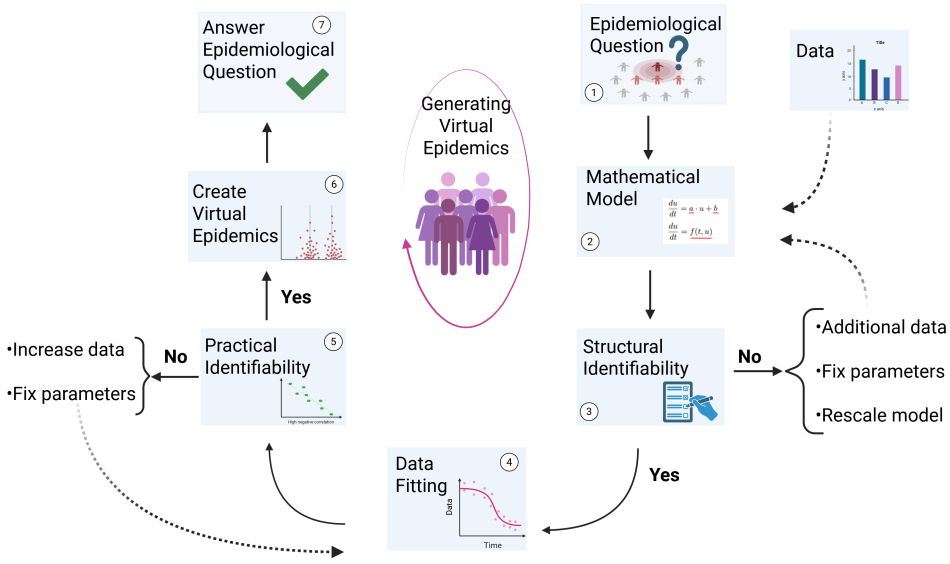

Figure 10. Schematic representation of generating VEs. Black arrows represent the initial process, and the dashed arrow represents iterative steps.

Table 11. MCS results: Model without PrEP.

Parameter	Λ	β	β_d	γ	γ_d
ARE					
$\sigma = 1\%$	0	0	0.1	0.1	7.8
ARE					
$\sigma = 5\%$	0.1	0.1	0.4	0.3	16.3
ARE					
$\sigma = 10\%$	0.1	0.1	0.8	0.6	22.8
ARE					
$\sigma = 20\%$	0.2	0.2	1.5	1.2	32.3

We generated VEs for the model without PrEP, as this model was both structurally and practically identifiable. Using the data-fitting approach, we generated VEs, producing a distribution of plausible epidemic trajectories relative to CDC-reported data. We began by estimating the variability in the HIV incidence data reported by the CDC, obtaining a standard deviation of $\sigma = 13.2$ for United States. HIV incidence. Using this estimate, we generated 1000 synthetic datasets by perturbing the empirical mean, with values constrained to lie within three standard deviations. Each synthetic dataset was then fit to the model, yielding an ensemble of plausible epidemic trajectories.

Table 12. MCS results: Model with PrEP and protection with fixed α.

Parameter	ω	χ	ψ	σ	ρ	γ	γ_d	β	β_d	q	Λ
ARE											
$\sigma = 1\%$	2.6	6.3	4.7	7.6	0.7	0.6	20.4	0.3	14.1	58.8	0.3
ARE											
$\sigma = 5\%$	2.4	4.1	4.2	10.1	1.4	1.1	38.8	0.8	41.4	63.6	0.6
ARE											
$\sigma = 10\%$	2.5	8.4	6.5	13.3	1.7	1.3	45.1	1	54.2	68.7	0.7
ARE											
$\sigma = 20\%$	2.4	5.4	7.1	17.9	2.3	1.5	48.8	1.2	63.2	75.3	1.7

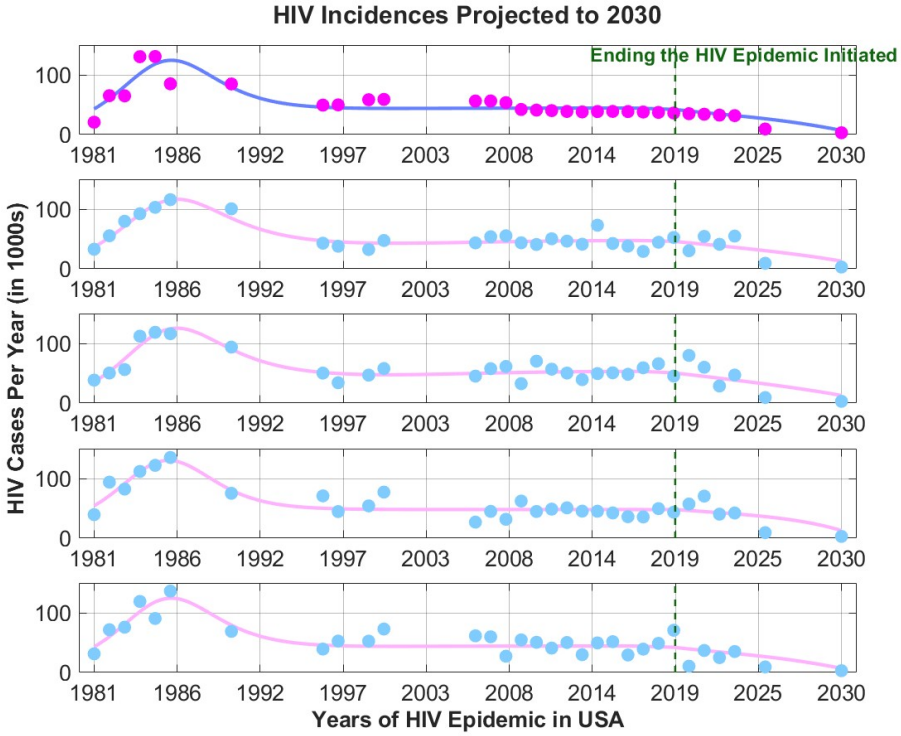

Figure 11. Individual trajectories of five VEs are shown in the subpanels. The first subpanel includes the actual data and the model solution curve, while the remaining panels display the simulated trajectories of four distinct VEs.

Figure 11 provides a detailed representation of VEs. The first subpanel displays the observed incidence data together with the model fit for reference, while the remaining subpanels show trajectories from four selected VEs that exhibit distinct qualitative behaviors. Figure 12 illustrates the model fit to annual HIV incidence data in the United States together with the resulting ensemble of virtual epidemic projections through 2030. Among these simulations, only 73 of 1000 VEs meet the 2030 target, corresponding to 7.3% success for the EHE initiative.

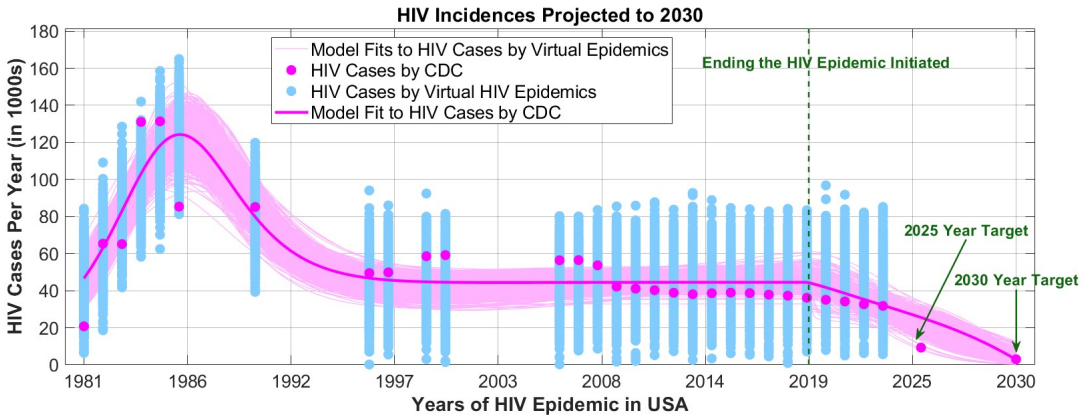

Figure 12. Model fitting and virtual epidemic simulations of annual HIV incidences in the United States, projected to 2030. A total of 1000 VEs are generated via bootstrapped parameter fitting. Light magenta curves represent model predictions for each virtual epidemic. Blue circles show VEs estimates of HIV cases from simulated datasets, while dark magenta circles and the solid magenta curve indicate the best fit to CDC-reported HIV incidence data. The vertical dashed line at 2019 marks the initiation of the EHE initiative. Arrows highlight the projected targets for 2025 and 2030.

5. Discussion

In this study, we examined the course of the HIV epidemic in the United States from 1981 to 2025 and projected potential epidemic trajectories through 2030 using two mathematical models: a transmission model and a transmission-behavior model. The transmission model captures the essential dynamics of HIV infection, diagnosis, treatment, and progression. The second model extends this framework to incorporate PrEP uptake through an evolutionary game-theoretic behavioral component, enabling prevention behavior to respond to epidemic conditions. Together, these models enable us to compare epidemic outcomes with and without PrEP and to determine how changes in prevention behavior influence the future course of the epidemic.

A central contribution of this work is the introduction of VEs, a new concept inspired by virtual patient populations used in pharmacokinetics to evaluate treatment strategies. Here, VEs were obtained by repeatedly fitting the model to bootstrapped surveillance data, generating a set of epidemic trajectories that were consistent with historical observations. This approach also helped clarify the uncertainty around long-term projections, which is important when these forecasts are used to assess progress toward public health goals.

Before generating VEs, we assessed the identifiability of our models. We began by evaluating the

structural identifiability of both models using the StructuralIdentifiability.jl package in Julia, to determine whether their parameters could, in principle, be uniquely determined from ideal data. For the model without PrEP, which was fit to CDC-estimated HIV incidence, all parameters were structurally identifiable once α and ρ were fixed. For the model with PrEP, which utilized three data sets: HIV incidence, the proportion of individuals using PrEP, and the number of AIDS classifications, structural identifiability was also achieved after fixing a small set of parameters. Thus, both models were structurally identifiable under some conditions.

We next validated the models by fitting them to the available surveillance data. For the model without PrEP, the fitting procedure used CDC-estimated HIV incidence, while the model with PrEP was fit to HIV incidence, PrEP use, and AIDS classifications. During data fitting, μ was fixed at 0.02 (a 50-year sexually active lifetime) to avoid unrealistically small estimates and to maintain biological plausibility. The parameters ρ and α were also fixed during the fitting procedure to ensure identifiability of the model parameters. We also imposed the constraints $\beta_d \leq \beta$ and $\gamma_d \leq \gamma$, consistent with the assumptions that treated individuals transmit at lower rates and progress to AIDS more slowly than untreated individuals. The fitted models were then used to project future epidemic trajectories and assess progress toward the EHE targets considered in this study.

We then assessed practical identifiability to evaluate the reliability of the estimated parameters, using a Monte Carlo simulation approach. For the model without PrEP, all parameters were practically identifiable, indicating that they could be estimated reliably from the available data. In contrast, the model with PrEP showed practical identifiability issues, with several parameters remaining unidentifiable even when multiple datasets were used. These findings suggest that the employed surveillance data do not contain enough information to estimate all parameters in the PrEP model reliably. As a result, we used the identifiable model without PrEP to generate VEs.

Using the model without PrEP, the virtual epidemic reproduced historical HIV incidence trends and generated a distribution of plausible future trajectories. Notably, only a small fraction (7.3%) of these trajectories achieved the EHE target of a 90% reduction in new infections by 2030. This suggests that, under current patterns of diagnosis, treatment, and prevention, the goal is unlikely to be met without additional intervention efforts. The spread of trajectories reflects the uncertainty in long-term epidemic forecasts, emphasizing the need for improved public health efforts. Because changes in PrEP uptake were not included, these projections represent epidemic dynamics without PrEP expansion.

The broader implication of this work is that VEs provide a flexible and informative framework for examining epidemic uncertainty and assessing national targets.

Use of AI tools declaration

The authors declare that they used Artificial Intelligence (AI) tools in the preparation of the introduction of this article. Specifically, Google Search and Google AI Overview were consulted during the literature review to obtain topic overviews and identify relevant references. All references were verified against the original source publications before inclusion in the manuscript.

Conflict of interest

Necibe Tuncer is a guest editor for Mathematical Biosciences and Engineering and was not involved in the editorial review or the decision to publish this article. All authors declare that there are no competing interests.

References

1. Canadian Foundation for AIDS Research, History of HIV/AIDS, 2026. Available from: https://canfar.com/awareness/about-hiv-aids/history-of-hiv-aids/.
2. N. R. Faria, A. Rambaut, M. A. Suchard, G. Baele, T. Bedford, M. J. Ward, et al., The early spread and epidemic ignition of HIV-1 in human populations, *Science*, **346** (2014), 56–61. https://doi.org/10.1126/science.1256739
3. HIV.gov, A timeline of HIV and AIDS, 2026. Available from: https://www.hiv.gov/hiv-basics/overview/history/hiv-and-aids-timeline.
4. World Health Organization, Why the HIV epidemic is not over, 2026. Available from: https://www.who.int/news-room/spotlight/why-the-hiv-epidemic-is-not-over.
5. HIVinfo.NIH.gov, HIV Treatment: The Basics, 2026. Available from: https://hivinfo.nih.gov/understanding-hiv/fact-sheets/hiv-treatment-basics.
6. I. D'Orso, C. V. Forst, Mathematical models of HIV-1 dynamics, transcription, and latency, *Viruses*, **15** (2023), 2119. https://doi.org/10.3390/v15102119
7. A. L. Hill, Mathematical models of HIV latency, in *HIV-1 Latency*, **417** (2017), 131–156. https://doi.org/10.1007/82_2017_77
8. A. S Perelson, R. M. Ribeiro, Modeling the within-host dynamics of HIV infection, *BMC Biol.*, **11** (2013), 96. https://doi.org/10.1186/1741-7007-11-96
9. W. Garira, A primer on multiscale modelling of infectious disease systems, *Infect. Dis. Modell.*, **3** (2018), 176–191. https://doi.org/10.1016/j.idm.2018.09.005
10. Centers for Disease Control and Prevention, Clinical Guidance for PrEP, 2026. Available from: https://www.cdc.gov/hivnexus/hcp/prep/index.html.
11. AIDSVu, PrEP Use Significantly Associated with Decreasing New HIV Diagnoses Across U.S. States, 2025. Available from: https://aidsvu.org/news-updates/prep-use-significantly-associated-with-decreasing-new-hiv-diagnoses-across-u-s-states.
12. A. T. Fojo, M. Schnure, P. Kasaie, D. W. Dowdy, M Shah, What will it take to end HIV in the United States? A comprehensive, local-level modeling study, *Ann. Intern. Med.*, **174** (2021), 1542–1553. https://doi.org/10.7326/m21-1501
13. Centers for Disease Control and Prevention, Estimated HIV Incidence and Prevalence, 2025. Available from: https://www.cdc.gov/hiv-data/nhss/estimated-hiv-incidence-and-prevalence.html.

14. P. S. Sullivan, M. Juhasz, S. N. DuBose, G. Le, K. Brisco, D. Islek, et al., Association of state-level PrEP coverage and new HIV diagnoses in the USA from 2012 to 2022: An ecological analysis of the population impact of PrEP, *Lancet HIV*, **12** (2025), 440–448. https://doi.org/10.1016/S2352-3018(25)00036-0

15. A. M. Bleichrodt, J. T. Okano, I. C. H. Fung, G. Chowell, S. Blower, The future of HIV: challenges in meeting the 2030 Ending the HIV Epidemic in the US (EHE) reduction goal, *AIDS*, **39** (2025), 708–718. https://doi.org/10.1097/QAD.0000000000004122

16. C. E. Lyons, O. J. Stokes-Cawley, A. Simkin, A. L. Bowring, I. M. Njindam, O. Njoya, et al., Modeling the potential impact of pre-exposure prophylaxis for HIV among men who have sex with men in Cameroon, *BMC Infect. Dis.*, **22** (2022), 751. https://doi.org/10.1186/s12879-022-07738-z

17. S. B. Kim, M. Yoon, N. S. Ku, M. H. Kim, J. E. Song, J. Y. Ahn, et al., Mathematical modeling of HIV prevention measures including pre-exposure prophylaxis on HIV incidence in South Korea, *PloS One*, **9** (2014), 90080. https://doi.org/10.1371/journal.pone.0090080

18. S. J. Gutowska, K. A. Hoffman, K. F. Gurski, The effect of PrEP uptake and adherence on the spread of HIV in the presence of casual and long-term partnerships, *Math. Biosci. Eng.*, **19** (2022), 11903–11934. https://doi.org/10.3934/mbe.2022555

19. L. Wang, N. Moqueet, A. Simkin, J. Knight, H. Ma, N. J. Lachowsky, et al., Mathematical modelling of the influence of serosorting on the population-level HIV transmission impact of pre-exposure prophylaxis, *AIDS*, **35** (2021), 1113–1125. https://doi.org/10.1097/QAD.0000000000002826

20. C. T. Bauch, Imitation dynamics predict vaccinating behaviour, *Proc. Biol. Sci.*, **272** (2005), 1669–1675. https://doi.org/10.1098/rspb.2005.3153

21. J. Yang, M. Martcheva, Y. Chen, Imitation dynamics of vaccine decision-making behaviours based on the game theory, *J. Biol. Dyn.*, **10** (2016), 31–58. https://doi.org/10.1080/17513758.2015.1099749

22. K. N. Nabi, K. M. A. Kabir, Modelling the dynamic vaccination game with evolutionary feedback: exploring pairwise interactions and vaccine strategies, *R. Soc. Open Sci.*, **11** (2024), 240460. https://doi.org/10.1098/rsos.240460

23. B. Wölfl, H. Rietmole, M. Salvioli, A. Kaznatcheev, F. Thuijsman, J. S. Brown, et al., The contribution of evolutionary game theory to understanding and treating cancer, *Dyn. Games Appl.*, **12** (2022), 313–342. https://doi.org/10.1007/s13235-021-00397-w

24. M. Craig, J. L. Gevertz, I. Kareva, K. P. Wilkie, A practical guide for the generation of model-based virtual clinical trials, *Front. Syst. Biol.*, **3** (2023), 1174647. https://doi.org/10.3389/fsysb.2023.1174647

25. A. Surendran, J. Le Sauteur-Robitaille, D. Kleimeier, J. Gevertz, K. Wilkie, A. L. Jenner, et al., Approaches to generating virtual patient cohorts with applications in oncology, in *Personalized Medicine Meets Artificial Intelligence*, (2023), 97–119. https://doi.org/10.1007/978-3-031-32614-1_8

26. T. R. Rieger, R. J. Allen, L. Bystricky, Y. Chen, G. W. Colopy, Y. Cui, et al., Improving the generation and selection of virtual populations in quantitative systems pharmacology models, *Prog. Biophys. Mol. Biol.*, **139** (2018), 15–22. https://doi.org/10.1016/j.pbiomolbio.2018.06.002
27. M. C. Luo, E. Nikolopoulou, J. L. Gevertz, From fitting the average to fitting the individual: A cautionary tale for mathematical modelers, *Front. Oncol.*, **12** (2022), 793908. https://doi.org/10.3389/fonc.2022.793908
28. Centers for Disease Control and Prevention, PrEP: A New Tool for HIV Prevention: August 2012, 2012. Available from: https://stacks.cdc.gov/view/cdc/13203.
29. J. Esparza, A brief history of the global effort to develop a preventive HIV vaccine, *Vaccine*, **31** (2013), 3502–3518. https://doi.org/10.1016/j.vaccine.2013.05.018
30. S. G. Sherman, D. Purchase, Point defiance: A case study of the United States' first public needle exchange in Tacoma, Washington, *Int. J. Drug Policy*, **12** (2001), 45–57. https://doi.org/10.1016/S0955-3959(00)00074-8
31. K. A. Bosh, H. I. Hall, L. Eastham, D. C. Daskalakis, J. H. Mermin, Estimated annual number of HIV infections-United States, 1981–2019, *Morb. Mortal. Wkly. Rep.*, **70** (2021), 801–806. http://doi.org/10.15585/mmwr.mm7022a1
32. Centers for Disease Control and Prevention, About AtlasPlus, 2026. Available from: https://www.cdc.gov/nchhstp/about/atlasplus.html.
33. America's HIV Epidemic Analysis Dashboard, Explore HIV Data in the U.S., 2026. Available from: https://ahead.hiv.gov.
34. N. Tuncer, M. Martcheva, S. M. Ciupe, Structural and practical identifiability of within-host models of virus dynamics-A review, *Curr. Opin. Syst. Biol.*, **42** (2025), 100552. http://doi.org/10.1016/j.coisb.2025.100552
35. R. Dong, C. Goodbrake, H. A. Harrington, G. Pogudin, Differential elimination for dynamical models via projections with applications to structural identifiability, *SIAM J. Appl. Algebra Geom.*, **7** (2023), 194–235. https://doi.org/10.1137/22M1469067
36. A. H. Peruski, B. Wu, L. Linley, K. P. Delaney, E. A. DiNenno, A. S. Johnson, Time from HIV infection to diagnosis in the U.S., 2014–2018, *Am. J. Prev. Med.*, **61** (2021), 636–643. https://doi.org/10.1016/j.amepre.2021.04.015
37. National Library of Medicine, June 5, 1981: The first report of AIDS in the U.S., 2021. Available from: https://circulatingnow.nlm.nih.gov/2021/06/04/june-5-1981-the-first-report-of-aids-in-the-u-s/.
38. B. J. Schmidt, J. A. Papin, C. J. Musante, Mechanistic systems modeling to guide drug discovery and development, *Drug Discovery Today*, **18** (2013), 116–127. https://doi.org/10.1016/j.drudis.2012.09.003
39. R. J. Allen, T. R. Rieger, C. J. Musante, Efficient generation and selection of virtual populations in quantitative systems pharmacology models, *CPT: Pharmacometrics Syst. Pharmacol.*, **5** (2016), 140–146. https://doi.org/10.1002/psp4.12063

40. Y. Cheng, C. J. Thalhauser, S. Smithline, J. Pagidala, M. Miladinov, H. E. Vezina, et al., QSP Toolbox: Computational implementation of integrated workflow components for deploying multi-Scale mechanistic models, *AAPS J.*, **19** (2017), 1002–1016. https://doi.org/10.1208/s12248-017-0100-x

41. N. Tuncer, H. Gulbudak, V. L. Cannataro, M. Martcheva, Structural and practical identifiability issues of immuno-epidemiological vector-host models with application to Rift Valley fever, *Bull. Math. Biol.*, **78** (2016), 1796–1827. https://doi.org/10.1007/s11538-016-0200-2

42. H. Miao, X. Xia, A. S. Perelson, H. Wu, On identifiability of nonlinear ODE models and applications in viral dynamics, *SIAM Rev.*, **53** (2011), 3–39. https://doi.org/10.1137/090757009

43. N. Tuncer, T. T. Le, Structural and practical identifiability analysis of outbreak models, *Math. Biosci.*, **299** (2018), 1–18. https://doi.org/10.1016/j.mbs.2018.02.004

44. A. Raue, J. Karlsson, M. P. Saccomani, M. Jirstrand, J. Timmer, Comparison of approaches for parameter identifiability analysis of biological systems, *Bioinformatics*, **30** (2014), 1440–1448. https://doi.org/10.1093/bioinformatics/btu006

45. Y. R. Liyanage, N. Heitzman-Breen, N. Tuncer, S. M. Ciupe, Identifiability investigation of within-host models of acute virus infection, *Math. Biosci. Eng.*, **21** (2024), 7394–7420. https://doi.org/10.3934/mbe.2024325

46. H. Wu, H. Zhu, H. Miao, A. S. Perelson, Parameter identifiability and estimation of HIV/AIDS dynamic models, *Bull. Math. Biol.*, **70** (2008), 785–799. https://doi.org/10.1007/s11538-007-9279-9

Appendix

A. Proof of Theorem 2.1

Proof. The Jacobian of the system is given by

$$J(E_0) = \begin{bmatrix} -\beta i + \beta i s - \beta_d t + \beta_d s t - \mu & -\beta s + \beta s i + \beta_d s t & -\beta_d s + \beta_d s t + \beta s i & 0 \\ \beta i - \beta i s + \beta_d t - \beta_d s t & \beta s - \beta s i - \beta_d s t - (\rho + \gamma + \mu) & \beta_d s - \beta_d s t - \beta s i & 0 \\ 0 & \rho & -\gamma_d - \mu & 0 \\ 0 & \gamma & \gamma_d & -\mu - \alpha \end{bmatrix},$$

where $s = \dfrac{S}{N}$, $i = \dfrac{I}{N}$, and $t = \dfrac{T}{N}$.

Since at the disease-free equilibrium, $s = 1, i = 0$, and $t = 0$, the Jacobian matrix of the system (2.3) at the disease-free equilibrium E_0 is

$$J(E_0) = \begin{bmatrix} -\mu & \beta & -\beta_d & 0 \\ 0 & \beta - (\rho + \gamma + \mu) & \beta_d & 0 \\ 0 & \rho & -\gamma_d - \mu & 0 \\ 0 & \gamma & \gamma_d & -\mu - \alpha \end{bmatrix}.$$

Among the four eigenvalues, two are $-\mu$ and $-\mu-\alpha$, both of which are negative. The remaining two are derived from the matrix J_1 below.

$$J_1 = \begin{bmatrix} \beta-(\rho+\gamma+\mu) & \beta_d \\ \rho & -\gamma_d-\mu \end{bmatrix}.$$

Now, we apply the criteria to ensure that the eigenvalues of J_1 have negative real parts. Specifically, we need $\mathrm{Tr}(J_1) < 0$ and $\mathrm{Det}(J_1) > 0$. The second condition leads to the following inequality

$$-(\beta-(\rho+\gamma+\mu))(\gamma_d+\mu)-\beta_d\rho > 0.$$

This inequality defines a reproduction number of the form,

$$\mathcal{R}_0 = \frac{\beta}{(\rho+\gamma+\mu)} + \frac{\beta_d\rho}{(\rho+\gamma+\mu)(\gamma_d+\mu)}.$$

We observe that the condition $\mathcal{R}_0 < 1$ ensures $\mathrm{Tr}(J_1) < 0$ and $\mathrm{Det}(J_1) > 0$. Therefore, when $\mathcal{R}_0 < 1$, the disease-free equilibrium is locally asymptotically stable. Conversely, if $\mathcal{R}_0 > 1$, the disease-free equilibrium becomes unstable. □

B. Proof of Theorem 2.2

Proof. To determine the endemic equilibrium E_1 for model (2.3), we set the right-hand side of system (2.3) to zero and obtain

$$\begin{aligned} 0 &= \Lambda - \beta\frac{S^*I^*}{N} - \beta_d\frac{S^*T^*}{N} - \mu S^*, \\ 0 &= \beta\frac{S^*I^*}{N} + \beta_d\frac{S^*T^*}{N} - (\rho+\gamma+\mu)I^*, \\ 0 &= \rho I^* - (\gamma_d+\mu)T^*, \\ 0 &= \gamma I^* + \gamma_d T^* - (\mu+\alpha)A^*. \end{aligned} \tag{B.1}$$

First, we solve for T^* using the third equation of system (B.1) and obtain

$$T^* = \frac{\rho I^*}{(\gamma_d+\mu)}. \tag{B.2}$$

Next, by solving for T^* in the third equation of system (B.1), we get

$$A^* = \frac{\gamma I^* + \gamma_d T^*}{(\mu+\alpha)},$$

Substitute T^* from Eq (B.2),

$$A^* = \frac{\gamma I^*}{(\mu+\alpha)} + \frac{\gamma_d\rho I^*}{(\mu+\alpha)(\gamma_d+\mu)}. \tag{B.3}$$

To determine N, by adding the first three equations of the system, we obtain

$$N^* = \frac{\Lambda}{\mu} - \frac{(\gamma I^* + \gamma_d T^*)}{\mu},$$

Substitute T^* from Eq (B.2),

$$N^* = \frac{\Lambda}{\mu} - \frac{1}{\mu}\left(\gamma + \frac{\gamma_d \rho}{\gamma_d + \mu}\right) I^*. \tag{B.4}$$

From the second equation of system (B.1) and Eq (B.2), we have

$$s = \frac{\gamma + \rho + \mu}{\left(\beta + \frac{\beta_d \rho}{\gamma_d + \mu}\right)} = \frac{1}{\mathcal{R}_0}, \tag{B.5}$$

where $s = \dfrac{S^*}{N^*}$.

From the first equation of system (B.1), we have

$$\Lambda - \beta s I^* - \frac{\beta_d \rho}{\gamma_d + \mu} s I^* - \mu N s = 0,$$

By substituting Eqs (B.4) and (B.5), we derive an equation for I^* as follows,

$$I^* = \frac{\Lambda\left(1 - \frac{1}{\mathcal{R}_0}\right)}{\mu + \gamma\left(1 - \frac{1}{\mathcal{R}_0}\right) + \rho\left(1 - \frac{\gamma_d}{\mathcal{R}_0(\gamma_d + \mu)}\right).} \tag{B.6}$$

If $\mathcal{R}_0 > 1$, it follows that $I^* > 0$ and is unique. Thus, the endemic equilibrium $E_1 = (S^*, I^*, T^*, A^*)$ is positive and unique when $\mathcal{R}_0 > 1$.

□

C. Proof of Theorem 2.3

Proof. The Jacobian matrix of system (2.3) at E_1 is

$$J(E_1) = \begin{bmatrix} -\beta i + \beta i s - \beta_d t + \beta_d s t - \mu & -\beta s + \beta s i + \beta_d s t & -\beta_d s + \beta_d s t + \beta s i & 0 \\ \beta i - \beta i s + \beta_d t - \beta_d s t & \beta s - \beta s i - \beta_d s t - (\rho + \gamma + \mu) & \beta_d s - \beta_d s t - \beta s i & 0 \\ 0 & \rho & -\gamma_d - \mu & 0 \\ 0 & \gamma & \gamma_d & -\mu - \alpha \end{bmatrix},$$

where $s = \dfrac{S^*}{N^*}$, $i = \dfrac{I^*}{N^*}$, and $t = \dfrac{T^*}{N^*}$.

It is clear that $-\mu - \alpha$ is an eigenvalue of the Jacobian $J(E_1)$ and it is negative. To find the remaining eigenvalues, we proceed by solving the characteristic equation of the Jacobian, J_2, below by setting $\mathrm{Det}|J_2 - \lambda| = 0$.

$$|J_2 - \lambda| = \begin{vmatrix} -\beta i + \beta i s - \beta_d t + \beta_d s t - \mu - \lambda & -\beta s + \beta s i + \beta_d s t & -\beta_d s + \beta_d s t + \beta s i \\ \beta i - \beta i s + \beta_d t - \beta_d s t & \beta s - \beta s i - \beta_d s t - (\rho + \gamma + \mu) - \lambda & \beta_d s - \beta_d s t - \beta s i \\ 0 & \rho & -\gamma_d - \mu - \lambda \end{vmatrix} = 0.$$

To simplify the expression, we perform the row operation of adding the second row to the first row of $|J_2 - \lambda|$, which gives

$$|J_2 - \lambda| = \begin{vmatrix} -\beta i + \beta is - \beta_d t + \beta_d st - \mu - \lambda & -\beta s + \beta si + \beta_d st & -\beta_d s + \beta_d st + \beta si \\ -\mu - \lambda & -(\rho + \gamma + \mu) - \lambda & 0 \\ 0 & \rho & -\gamma_d - \mu - \lambda \end{vmatrix} = 0.$$

Expanding the determinant, we obtain the following equation

$$\begin{aligned} 0 = (-\beta i + \beta is - \beta_d t + \beta_d st - \mu - \lambda)\,((-\rho - \gamma - \mu - \lambda)(-\gamma_d - \mu - \lambda)) + \\ (\beta s - \beta si - \beta_d st)(-\mu - \lambda)(-\gamma_d - \mu - \lambda) - (\beta_d s - \beta_d st - \beta si)(-\mu - \lambda)\rho. \end{aligned} \tag{C.1}$$

Rearranging the terms in the equation above, we get

$$\begin{aligned} &(\beta i - \beta is + \beta_d t - \beta_d st + \mu + \lambda)\,((\rho + \gamma + \mu + \lambda)(\gamma_d + \mu + \lambda)) \\ &= (\beta s - \beta si - \beta_d st)(\mu + \lambda)(\gamma_d + \mu + \lambda) + (\beta_d s - \beta_d st - \beta si)(\mu + \lambda)\rho. \end{aligned}$$

Here, we assume $\beta \geq \beta_d$, which implies $\beta s(1 - i) - \beta_d st \geq \beta s(1 - i - t) > 0$.

After simplification we obtain

$$\begin{aligned} &(\beta i + \beta_d t - \beta_d st + \mu + \lambda)(\lambda + \mu + \rho + \gamma)(\lambda + \mu + \gamma_d) - \beta si\gamma(\lambda + \mu + \gamma_d) - \rho\beta si\gamma_d \\ &= \rho(\beta_d s - \beta_d st)(\lambda + \mu) + (\beta s - \beta_d st)(\lambda + \mu)(\lambda + \mu + \gamma_d). \end{aligned}$$

We divide by $(\lambda + \mu)(\lambda + \mu + \gamma_d)(\lambda + \mu + \rho + \gamma)$ and get

$$\begin{aligned} &\frac{\beta i + \beta_d t - \beta_d st + \mu + \lambda}{\lambda + \mu} - \frac{\beta si\gamma}{(\lambda + \mu)(\lambda + \mu + \rho + \gamma)} - \frac{\rho\beta si\gamma_d}{(\lambda + \mu)(\lambda + \mu + \gamma_d)(\lambda + \mu + \rho + \gamma)} \\ &= \frac{\rho(\beta_d s - \beta_d st)}{(\lambda + \mu + \rho + \gamma)(\lambda + \mu + \gamma_d)} + \frac{(\beta s - \beta_d st)}{(\lambda + \mu + \rho + \gamma)}. \end{aligned} \tag{C.2}$$

To prove the stability of the endemic equilibrium, the goal is to show that all eigenvalues of Eq (C.1) have negative real parts. We use a method of contradiction by assuming the existence of an eigenvalue λ, such that $Re(\lambda) \geq 0$.

Considering the numerator of the left side of Eq (C.2), we have

$$= \left| A + x + y\mathbf{i} - \beta is \frac{\left(\gamma + \rho\frac{\gamma_d(x + \mu + \gamma_d)}{(x + \mu + \gamma_d)^2 + y^2}\right)(x + \mu + \rho + \gamma) - \frac{\rho\gamma_d y^2}{(x + \mu + \gamma_d)^2 + y^2} - By\mathbf{i}}{(x + \mu + \gamma + \rho)^2 + y^2} \right|,$$

where $A = \beta i + \beta_d - \beta_d st + \mu$ and $B = \gamma + \rho\frac{\gamma_d(x + \mu + \gamma_d)}{(x + \mu + \gamma_d)^2} + (x + \mu + \rho + \gamma)\frac{\rho\gamma_d}{(x + \mu + \gamma_d)^2 + y^2}$, and $\mathbf{i}$ denotes the imaginary unit. We note that $B > 0$.

$$= \left| A + x - \beta is \frac{\left(\gamma + \rho\frac{\gamma_d(x + \mu + \gamma_d)}{(x + \mu + \gamma_d)^2 + y^2}\right)(x + \mu + \rho + \gamma) - \frac{\rho\gamma_d y^2}{(x + \mu + \gamma_d)^2 + y^2}}{(x + \mu + \gamma + \rho)^2 + y^2} + y\mathbf{i}(1 + \beta isB) \right|.$$

Consider

$$\beta i - \beta is\frac{\left(\gamma + \rho\frac{\gamma_d(x+\mu+\gamma_d)}{(x+\mu+\gamma_d)^2+y^2}\right)(x+\mu+\rho+\gamma) - \frac{\rho\gamma_d y^2}{(x+\mu+\gamma_d)^2+y^2}}{(x+\mu+\gamma+\rho)^2+y^2} >$$

$$\beta i - \beta is\frac{\left(\gamma + \rho\frac{\gamma_d(x+\mu+\gamma_d)}{(x+\mu+\gamma_d)^2+y^2}\right)(x+\mu+\rho+\gamma)}{(x+\mu+\gamma+\rho)^2+y^2} \geq \beta i - \beta is\frac{(\gamma+\rho)(x+\mu+\rho+\gamma)}{(x+\mu+\rho+\gamma)^2+y^2} \geq \beta i - \beta is \geq 0.$$

Thus,

$$A - \beta isQ > \mu,$$

where $Q = \dfrac{\left(\gamma + \rho\frac{\gamma_d(x+\mu+\gamma_d)}{(x+\mu+\gamma_d)^2+y^2}\right)(x+\mu+\rho+\gamma) - \frac{\rho\gamma_d y^2}{(x+\mu+\gamma_d)^2+y^2}}{(x+\mu+\gamma_+\rho)^2+y^2}$.

This implies,

$$\frac{(x+A-\beta isQ)^2 + y^2(1+\beta isB)^2}{(x+\mu)^2+y^2} > 1.$$

This means that for λ with $Re(\lambda) \geq 0$, the left-hand side of Eq (C.2) is always greater than 1.

By considering the right-hand side of the Eq (C.2), we can show that

$$\left|\frac{(\beta s - \beta si)(\gamma_d+\mu+\lambda) + (\beta_d s - \beta_d st)\rho}{(\rho+\gamma+\mu+\lambda)(\gamma_d+\mu+\lambda)}\right| \leq \left|\frac{(\beta s - \beta si)}{(\rho+\gamma+\mu+\lambda)}\right| + \left|\frac{(\beta_d s - \beta_d st)\rho}{(\rho+\gamma+\mu+\lambda)(\gamma_d+\mu+\lambda)}\right|$$

$$\leq \left|\frac{\beta s}{(\rho+\gamma+\mu+\lambda)}\right| + \left|\frac{\beta_d s\rho}{(\rho+\gamma+\mu+\lambda)(\gamma_d+\mu+\lambda)}\right|.$$

From the second equation of system (B.1),

$$\frac{\beta sI^* + \beta_d sT^*}{(\rho+\gamma+\mu)I^*} = 1.$$

Since $\dfrac{\rho}{(\gamma_d+\mu)} = \dfrac{T^*}{I^*}$ by the third equation of the system, (B.1), we obtain

$$\frac{\beta s}{(\rho+\gamma+\mu+\lambda)} + \frac{\beta_d s\rho}{(\rho+\gamma+\mu+\lambda)(\gamma_d+\mu+\lambda)} = 1,$$

Which implies that the right hand side of the Eq (C.2) is less than one. That is,

$$\left|\frac{(\beta s - \beta si)(\gamma_d+\mu+\lambda) + (\beta_d s - \beta_d st)\rho}{(\rho+\gamma+\mu+\lambda)(\gamma_d+\mu+\lambda)}\right| \leq 1.$$

This contradicts our earlier result that the left-hand side is always greater than 1. Thus, the eigenvalues of characteristic equation (C.1) have negative real parts, completing the proof of the theorem. □

D. Practical identifiability analysis

Practical identifiability assesses whether model parameters can be reliably recovered from noisy and limited experimental data. Unlike structural identifiability, which is determined purely by the model's structure, inputs, and measured outputs, practical identifiability depends explicitly on the quality and quantity of available data. Several mathematical tools have been developed to evaluate practical identifiability, such as the fisher information matrix (FIM), Profile Likelihood Method, and Bayesian Methods [41–46]. In this study, we focused on a Monte Carlo simulation approach [41–43].

We performed Monte Carlo simulations by generating 1000 synthetic datasets using the estimated parameters as the true parameter set $\hat{p}$. Measurement noise was added at increasing levels. The simulation procedure followed the steps below:

1) The model was numerically solved using the true parameter set $\hat{p}$, and the corresponding model outputs were recorded at the experimental time points.

2) A total of 1000 synthetic datasets were generated from the model by adding normally distributed noise with mean 0 and standard deviation σ, where σ represents the measurement noise level (1%, 5%, 10%, 20%).

3) For each synthetic dataset, parameter set p_q was obtained by fitting the model.

4) The average relative estimation error (ARE) for each parameter is calculated as

$$\mathrm{ARE}(p^{(k)}) = 100\% \times \frac{1}{M}\sum_{q=1}^{M}\frac{\left|\hat{p}^{(k)} - p_q^{(k)}\right|}{\left|\hat{p}^{(k)}\right|},$$

where $\hat{p}^{(k)}$ denotes the true parameter and $p_q^{(k)}$ is its estimate from the qth data set.

5) Steps 1)–4) were repeated for noise levels $\sigma = 1\%, 5\%, 10\%, 20\%$.

Definition D.1. *The practical identifiability of a parameter p is determined by comparing its ARE with the measurement error σ.*

- *If $0 \le ARE(p) \le \sigma$, then, parameter p is considered (strongly) practically identifiable.*
- *If $\sigma < ARE(p) \le 10\sigma$, then p is weakly practically identifiable.*
- *If $ARE(p) > 10\sigma$, then p is practically unidentifiable.*

We applied the MCS method to both models: the model without PrEP and the model with PrEP. The results are presented in Tables 11 and 12, respectively. According to the results for the model without PrEP, parameters Λ, β, β_d, and γ are strongly practically identifiable, whereas parameter γ_d is weakly practically identifiable. For the model with PrEP, practical identifiability was observed only for parameters $\omega, \chi, \psi, \sigma, \gamma, \rho, \beta$, and Λ. All remaining parameters could not be reliably estimated.

AIMS Press